ARFLOW: AUTO-REGRESSIVE OPTICAL FLOW ESTIMATION FOR ARBITRARY-LENGTH VIDEOS VIA PROGRESSIVE NEXT-FRAME FORECASTING

Jiuming Liu[1*], **Mengmeng Liu**[2*], **Siting Zhu**[1], **Yunpeng Zhang**[3], **Jiangtao Li**[3], **Michael Ying Yang**[4], **Francesco Nex**[2], **Hao Cheng**[2†], **Hesheng Wang**[1†]
[1]Shanghai Jiao Tong University [2]University of Twente [3]Phigent Robotics [4]University of Bath
liujiuming123@gmail.com, m.liu-1@utwente.nl

ABSTRACT

Optical flow estimation is a fundamental computer vision task that predicts per-pixel displacements from consecutive images. Recent works attempt to exploit temporal cues to improve the estimation performance. However, their temporal modeling is restricted to short video sequences due to the unaffordable computational burden, thereby suffering from restricted temporal receptive fields. Moreover, their group-wise paradigm in one forward pass undermines inter-group information exchange, leading to modest performance improvement. To address these problems, we propose a novel multi-frame optical flow network based on an auto-regressive paradigm, named ARFlow. Unlike previous multi-frame methods, our method can be scalable to arbitrary-length videos with marginal computational overhead. Specifically, we design an Auto-regressive Flow Initialization (AFI) module and an Auto-regressive Multi-stride Flow Refinement (AMFR) module to forecast the next-frame flow based on multi-stride history observations. Our ARFlow achieves state-of-the-art performance, ranking 1st on both KITTI-2015 and Spring official benchmarks and 2nd on the MPI-Sintel (Final) benchmark among all open-sourced methods. Furthermore, due to the auto-regressive nature, our method can generalize to arbitrary video length with a constant GPU memory usage of 2.1GB.

1 INTRODUCTION

Optical flow indicates the 2D displacement field of each pixel predicted from consecutive video frames, playing a key role in various downstream applications such as video inpainting (Xu et al., 2019; Li et al., 2022), dynamic scene reconstruction (LU et al., 2025; Zhu et al., 2024; Deng et al., 2025b; Chan et al., 2026; Li et al., 2023), and video generation (Liang et al., 2024a;b).

With the development of advanced model architectures (Deng et al., 2025c), optical flow estimation has witnessed remarkable success, evolving from CNN-based backbones (Sun et al., 2018a; Teed & Deng, 2020) to transformer-based ones (Huang et al., 2022; Xu et al., 2022); from discriminative methods (Zhao et al., 2024) to generative ones (Luo et al., 2024; Saxena et al., 2023; Liu et al., 2024a; 2025c). However, these methods typically formulate the task with a pairwise paradigm, which neglects intrinsic temporal coherence within video sequences, leading to suboptimal performance and poor reasoning ability in occluded areas (Chen et al., 2023; Dong & Fu, 2024; Liu et al., 2023c).

Recently, there has been an increasing research focus on multi-frame optical flow estimation from video sequences (Shi et al., 2023a; Sun et al., 2024; Bargatin et al., 2025; Dong & Fu, 2024), as shown in Fig. 1. However, we observe that concurrent multi-frame methods commonly fail to exploit sufficient temporal cues because of the following: (1) *Limited temporal receptive fields:* Existing multi-frame settings typically segment the entire video into multiple groups with a fixed size, e.g., three frames in MemFlow (Dong & Fu, 2024) (Fig. 1 (A)), four frames in StreamFlow (Sun et al., 2024) (Fig. 1 (B)). This group-wise segmentation fails to capture long-range dependencies

[*]These authors contributed equally. [†]Corresponding authors: Hao Cheng, Hesheng Wang.

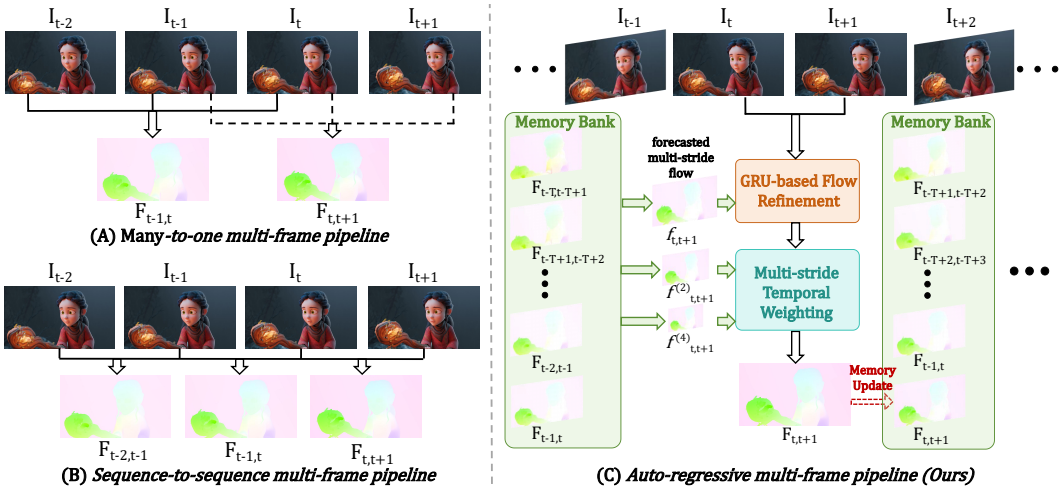

Figure 1: Comparison with previous multi-frame optical flow methods.

throughout the total video length. (2) *Heavy computational overhead and memory usage:* VideoFlow (Shi et al., 2023a) inputs overlapping clips to estimate multiple flows. MemFlow (Dong & Fu, 2024) utilizes many image inputs to strengthen the current estimation. Both approaches repeat feature extraction and context encoder several times in different groups, impeding real-time applications. StreamFlow (Sun et al., 2024) suffers from high GPU memory usage, as shown in Fig. 2. This inefficiency further leads to poor scalability, allowing only a limited number of frame inputs. (3) *Lack of multi-stride temporal modeling:* Prior methods typically focus on single-stride temporal modeling with short-term motions. However, both long-range and short-term motions are crucial for optical flow: long-range motions facilitate recognizing occlusions and out-of-boundary pixels across frames (Shi et al., 2023a), while short-term motions capture subtle variations in adjacent frames.

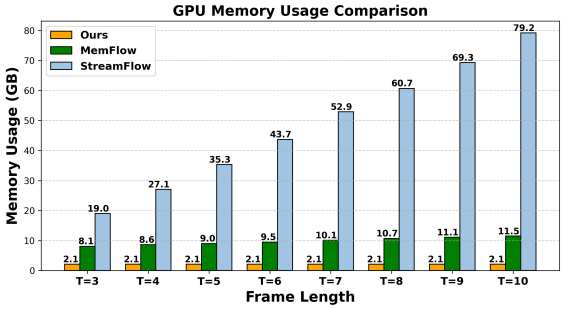

Figure 2: Previous group-wise multi-frame methods suffer from a significant memory usage increase with longer frame length. In contrast, our method maintains nearly constant GPU consumption.

To address these problems, we propose a novel multi-frame optical flow estimation pipeline (ARFlow) using an auto-regressive prediction paradigm in Fig. 1 (C). Specifically, an Auto-regressive Flow Initialization module (AFI) is developed to retrieve multiple history flow estimates from the memory bank and forecast the next-frame initial flow based on the history ones. This process will introduce an accurately initialized flow, which significantly improves the performance and also decreases the iteration numbers in subsequent refinement modules, enabling higher efficiency. After obtaining the initial flow, another Auto-regressive Multi-stride Flow Refinement module (AMFR) is also designed by incorporating multi-granularity temporal information from diverse intervals to combine both long-term and short-term motions. Unlike previous multi-frame works that segment videos into multiple groups, we utilize the entire video sequence as the network input, where sequential images are delivered frame by frame. When a new frame is input, its features are extracted and correlated with previous history flows to predict the current flow. This paradigm breaks the limitation of local receptive fields, possessing strong scalability to arbitrary frame lengths with no memory usage increase in Fig. 2. **Please refer to the supplementary videos for scalable optical flow estimation on arbitrary-length inputs.**

Overall, the main contributions of our method are as follows:

- We design a novel multi-frame optical flow estimation method, named ARFlow, based on the auto-regressive paradigm. Through progressively forecasting the next-frame flow, our method can be scalable to arbitrary-length videos.

- An Auto-regressive Flow Initialization module (AFI) is developed to retrieve multiple history flows from memory banks and forecast the next-frame initial flow based on these history estimates.
- An Auto-regressive Multi-stride Flow Refinement module (AMFR) is also designed to further refine the initial flow by incorporating both long-term and short-term temporal cues.
- Extensive experiments on MPI-Sintel (Butler et al., 2012), Spring (Mehl et al., 2023b), and KITTI-2015 (Geiger et al., 2013) datasets demonstrate the state-of-the-art performance of our proposed ARFlow. Moreover, due to the accurately predicted initial flows, the number of iterations in the following refinement module is decreased, enabling lower memory usage compared with prior multi-frame methods.

2 Related Work

Pairwise Optical Flow Estimation. Traditional methods (Black & Anandan, 1993; Bruhn et al., 2005; Horn & Schunck, 1981) typically formulate optical flow estimation as an optimization problem which maximizes the visual similarity between two frames. FlowNet (Dosovitskiy et al., 2015) regresses the optical flow with Convolutional Neural Networks (CNNs) in an end-to-end manner. PWC-Net (Sun et al., 2018b) proposes a Pyramid, Warping, Cost volume method for coarse-to-fine flow estimations. To address the problem of small fast-moving objects, RAFT (Teed & Deng, 2020) designs a recurrent iteration module to improve estimation accuracy. Subsequent works (Ranjan & Black, 2017; Hui et al., 2018; Yang & Ramanan, 2019; Hui et al., 2020; Jiang et al., 2021; Zhang et al., 2021; Sun et al., 2022; Jahedi et al., 2023; Wang et al., 2024b) progressively refine model architectures in a coarse-to-fine or iterative manner. Various transformer-based methods (Huang et al., 2022; Shi et al., 2023b; Xu et al., 2022; Liu et al., 2023b; Shan et al., 2021; Sui et al., 2022; Luo et al., 2023) are then developed to enlarge the matching receptive field. Some methods Liu et al. (2022; 2023a) also incorporate scene flow estimation Jiang et al. (2024); Liu et al. (2025d); Zhang et al. (2024); Liu et al. (2025b); Zhang et al. (2025); Liu et al. (2024c;b); Feng et al. (2024) by joint optimization. Nevertheless, these two-frame optical flow methods fail to take intrinsic temporal cues across frames into consideration.

Multi-Frame Optical Flow Estimation. The research for multi-frame flow estimation has gained remarkable advances in recent years. RAFT (Teed & Deng, 2020) utilizes a "warm-start" strategy, which initializes the current flow by warping previous flow estimates. Some self-supervised methods (Liu et al., 2019; Hur & Roth, 2021) are also proposed to retrieve temporal information by CNN or LSTM. VideoFlow (Shi et al., 2023a) calculates the bi-directional flows with a three-frame setting and designs a motion propagation module to exchange information across different triplets. SplatFlow (Wang et al., 2024a) introduces a differential splatting transformation to align motion features from previous timestamps. StreamFlow (Sun et al., 2024) proposes an in-batch estimation strategy, simultaneously estimating all successive flows. More recently, memory mechanisms (Dong & Fu, 2024; Bargatin et al., 2025) have been introduced to store previous flow-related features and further improve the current estimation. However, these prior multi-frame methods can only process segmented groups with limited sizes (3-5 frames), impeding sufficient temporal modeling. Also, they suffer from heavy computational burdens and memory usage with increasing video lengths. In this paper, our ARFlow resorts to the auto-regressive transformer by progressively forecasting the next frame's motion, which is scalable to arbitrary video lengths while keeping low memory usage.

Auto-regressive Video Generation. Recently, auto-regressive models benefiting from scaling laws (Henighan et al., 2020) have gained great success in the video generation field (Xie et al., 2025; Yin et al., 2025; Tang et al., 2024; Zhou et al., 2025; Henschel et al., 2025; Zhai et al., 2025; Huang et al., 2025; Liu et al., 2025a; Deng et al., 2025a; Liu et al., 2025e; Ge et al., 2026; Xu et al., 2024). PA-VDM Xie et al. (2025) proposes a progressive noise-adding mechanism and denoises the frame using small intervals. CausVID Yin et al. (2025) adapts a pre-trained bidirectional transformer and designs a distribution matching distillation technique to reduce latency. Self Forcing Huang et al. (2025) presents the auto-regressive rollout with key-value (KV) caching during training. Recent studies have also emphasized temporal structure and long-horizon dependencies for dynamic-scene understanding (Liu et al., 2025f; 2024d; 2023d; Cheng et al., 2023b;a), motivating an auto-regressive formulation for optical flow. Inspired by the great success in these auto-regressive video generation works, we, for the first time, introduce the auto-regressive paradigm into optical flow estimation.

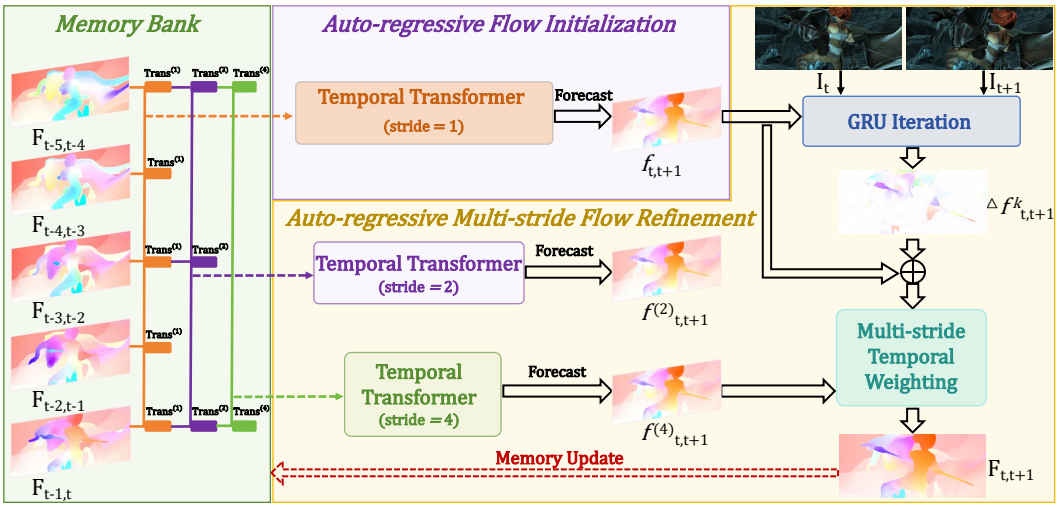

Figure 3: The overall architecture of our proposed ARFlow.

3 METHOD

3.1 OVERALL ARCHITECTURE

As in Fig. 1 (C), the input of our network is a video sequence $I_1, I_2, ..., I_{L-1}, I_L$, where $I_t \in H \times W \times 2$ indicates the image at the timestamp t. H, W are the height and width of the input images. The outputs are corresponding sequential optical flows $F_{1,2}, F_{2,3}, ..., F_{L-1,L}$ between consecutive image pairs, where $F_{t,t+1}$ indicates the optical flow from I_t to I_{t+1}.

In our auto-regressive setting, sequential images are delivered into the network frame by frame. When a new frame I_{t+1} is inputted into Fig. 3, a forecasted flow initialization $f_{t,t+1}$ is first generated based on previously predicted T frames' history flows stored in the memory bank in Section 3.2. Then, above initial flow $f_{t,t+1}$ is iteratively refined by incorporating intermediate context and motion features from I_t to I_{t+1} and multi-stride forecasted flows in Section 3.3. The output refined flow is finally used to update the memory bank and forecast the following flow $f_{t+1,t+2}$ in an auto-regressive manner. The network is supervised by the loss functions defined in Section 3.4.

3.2 AUTO-REGRESSIVE FLOW INITIALIZATION

Motivated by prior works from Xu et al. (2023a), long-range temporal dependencies are crucial for optical flow estimation, where potential challenges such as occlusions can be alleviated utilizing multi-frame temporal cues. In addition, optical flows for dynamic objects tend to be consistent across frames. Therefore, we use history flow estimates from a designed memory bank to forecast an extrapolated flow in the next frame for enhanced flow initialization.

Memory Bank. When a new pair of images (I_t and I_{t+1}) is delivered to the network as in Fig. 3, our method first forecasts the intermediate initial flow based on historically predicted flows. To effectively store multiple history flows, we design a memory bank with a fixed length T, which stores the nearest T frames' predicted flows $\{F_{i,i+1}\}_{i=t-T}^{t-1}$. When the number of predicted flows is less than T, the first several frames' flows are directly stored in the memory bank as memory initialization. The memory bank is maintained by a sliding window mechanism: When a new flow is predicted, it is stored in the memory bank, and the temporally-farthest one is discarded. To guarantee efficiency, our stored flows are at the 1/16 resolution of the original image size.

Auto-regressive Next-Frame Forecasting. For the intermediate optical flow estimation, we predict the next-frame flow based on previously stored flows as:

$$\{\mathbf{Feat}_i^{(1)}\}_{i=t-T}^{t-1} = \mathrm{Trans}^{(1)}\left(\{F_{i,i+1}\}_{i=t-T}^{t-1}\right), \quad f_{t,t+1} = \phi(\mathbf{Feat}_{t-1}^{(1)}), \tag{1}$$

where $\mathrm{Trans}^{(1)}$ is a transformer encoder for temporal modeling on all input frames, $\phi(\cdot)$ is a lightweight Conv2d projection, and $f_{t,t+1}$ denotes the initial flow predicted from the last token

$\mathbf{Feat}_{t-1}^{(1)}$. Since this initial flow predicted from multiple history flows possesses the long-range temporal cues, it can provide an enhanced flow initialization.

3.3 AUTO-REGRESSIVE MULTI-STRIDE FLOW REFINEMENT

After getting the initial flow $f_{t,t+1}$, we further leverage GRU-based iterations based on current observations and multi-stride history weighting to refine $f_{t,t+1}$. Notably, both refinements are conducted at the 1/16 of original resolution for fast inference.

GRU-based Iterative Refinement. We first leverage a GRU-based refinement to incorporate the information derived from current input images I_t, I_{t+1}. Specifically, the feature maps E_t, E_{t+1} of current image pairs are first extracted by ResNet16 (He et al., 2016). Then, we obtain the intermediate context feature from the current images as:

$$c, h^0 = \mathrm{ContextNetwork}(I_t, I_{t+1}), f^0 = \mathrm{FlowHead}(h^0), \tag{2}$$

where $\mathrm{ContextNetwork}$ follows the setting in (Bargatin et al., 2025). c and h^0 respectively indicate the context feature and the initial hidden state in GRU. f^0 is the predicted intermediate flow. If there are no stored history flows (the first image pairs), we use f^0 as the input of GRU. Otherwise, we use the temporally forecasted flow $f_{t,t+1}$ as the input flow in GRU as:

$$f_{t,t+1}^0 = \begin{cases} f^0, & when\ t = 0\ ; \\ f_{t,t+1}, & otherwise\ , \end{cases} \tag{3}$$

where $f_{t,t+1}^0$ is the input initial flow of the GRU module. Also, we associate two frames to obtain a correlation feature map $V(u,v) =< E_t(u), E_{t+1}(v) >$, where $< \cdot, \cdot >$ denotes the dot product. u, v denote the u-th and v-th element respectively in E_t and E_{t+1}. For the k-th iteration, the correlation values are retrieved by the look-up operation from V based on updated flow as: $V^k = \mathrm{LookUp}(V, f_{t,t+1}^{k-1})$, where $f_{t,t+1}^{k-1}$ is the intermediate output flow from the (k-1)-th iteration. Then, the intermediate motion feature M^k is generated by $M^k = \mathrm{MotionEncoder}(\mathrm{MLP}(V^k), \mathrm{MLP}(f_{t,t+1}^{k-1}))$. Finally, the hidden state is iteratively updated by combining context feature c, motion feature M^k, and the previous hidden state $h^k = \mathrm{GRU}(c, M^k, h^{k-1})$. Afterwards, the intermediate residual flows are obtained from the updated hidden state $\Delta f_{t,t+1}^k = \mathrm{FlowHead}(h^k)$. The output flow after the k-th iteration is generated by per-point adding between the intermediate residual flow and initial flow as:

$$f_{t,t+1}^k = f_{t,t+1}^{k-1} + \Delta f_{t,t+1}^k. \tag{4}$$

We repeat the above process for K times to generate the final refined flow $f_{t,t+1}^K$ after GRU.

Multi-stride Temporal Weighting Refinement. The above GRU-based iterations only incorporate the context and motion features from the current timestamp, without consideration of multi-stride history flows or motions. This leads to poor adaptation to various motion variations. To address the problem, we continually refine $f_{t,t+1}^K$ with multi-stride temporal forecasting.

Because the low-frequency and high-frequency information displays with unpredictable patterns along the entire video length, the single-stride temporal modeling in Section 3.2 is not effective enough to capture long-range motion variations. To enlarge the temporal receptive field and strengthen the adaptation ability to diverse motion variations, we also generate forecasted flows by the multi-stride temporal modeling in a cascaded manner. Specifically, we further sample frames with strides of 2 and 4 as:

$$\{\mathbf{Feat}_i^{(2)}\}_{i\in\{t-1,\,t-3,\,\dots\}} = \mathrm{Trans}^{(2)}\Big(\{\mathbf{Feat}_i^{(1)}\}_{i\in\{t-1,\,t-3,\,\dots\}}\Big), \quad f_{t,t+1}^{(2)} = \phi(\mathbf{Feat}_{t-1}^{(2)}) \tag{5}$$

$$\{\mathbf{Feat}_i^{(4)}\}_{i\in\{t-1,\,t-5,\,\dots\}} = \mathrm{Trans}^{(4)}\Big(\{\mathbf{Feat}_i^{(2)}\}_{i\in\{t-1,\,t-5,\dots\}}\Big), \quad f_{t,t+1}^{(4)} = \phi(\mathbf{Feat}_{t-1}^{(4)}) \tag{6}$$

$$\{\mathbf{Feat}_{\text{fuse}}^{(l)}\}_{l\in\{1,\,2,\,4\}} = \mathrm{Trans}^{(f)}\Big(\mathbf{Feat}_{t-1}^{(1)}, \mathbf{Feat}_{t-1}^{(2)}, \mathbf{Feat}_{t-1}^{(4)}\Big), \quad f_{\text{fuse}} = \phi(\mathbf{Feat}_{\text{fuse}}^{(4)}), \tag{7}$$

where $\mathrm{Trans}^{(2)}$ and $\mathrm{Trans}^{(4)}$ perform temporal modeling with stride 2 and stride 4, and $\mathrm{Trans}^{(f)}$ aggregates multi-stride features. Both $f_{t,t+1}^{(2)}$ and $f_{t,t+1}^{(4)}$ are used as auxiliary supervision in the

Table 1: **Benchmark results on MPI-Sintel and KITTI-15.** We report endpoint-error (EPE) on Sintel (Butler et al., 2012) and Fl on KITTI-15 (Geiger et al., 2013).

	Method	Reference	Sintel Clean			Sintel Final			KITTI-15	
			Mat.↓	Unm.↓	All↓	Mat.↓	Unm.↓	All↓	All↓	Non-Occ↓
Pairwise	FlowNet2 (Ilg et al., 2017b)	CVPR'17	1.56	25.40	4.16	2.75	30.11	5.74	10.41	6.94
	PWC-Net (Sun et al., 2018b)	CVPR'18	1.45	23.47	3.86	2.44	27.08	5.04	9.60	6.12
	RAFT (Teed & Deng, 2020)	ECCV'20	0.62	9.65	1.61	1.41	14.68	2.86	5.10	3.07
	GMFlow (Xu et al., 2022)	CVPR'22	0.65	10.56	1.74	1.32	15.80	2.90	9.32	3.80
	FlowFormer (Huang et al., 2022)	CVPR'22	0.42	7.16	1.16	0.96	11.30	2.09	4.68	2.69
	GMFlow+ (Xu et al., 2023b)	TPAMI'23	**0.34**	6.68	1.03	1.10	12.74	2.37	4.49	2.40
	Flowformer++ (Shi et al., 2023b)	CVPR'23	0.39	6.64	1.07	0.88	10.63	1.94	4.52	-
	AnyFlow (Jung et al., 2023)	CVPR'23	0.42	7.68	1.21	1.12	13.37	2.44	4.41	2.69
	CroCoFlow (Weinzaepfel et al., 2023)	ICCV'23	0.39	6.85	1.09	1.21	12.42	2.44	3.64	2.40
	DDVM (Saxena et al., 2023)	NeurIPS'23	0.83	9.26	1.75	1.28	12.20	2.48	3.26	2.24
	FlowDiffuser (Luo et al., 2024)	CVPR'24	0.38	6.23	1.02	0.97	10.67	2.03	4.17	2.82
	SEA-RAFT(L) (Wang et al., 2024b)	ECCV'24	0.44	8.40	1.31	1.20	14.06	2.60	4.30	-
	SAMFlow (Zhou et al., 2024)	AAAI'24	0.38	5.97	1.00	1.04	10.60	2.08	4.49	-
	DPFlow (Morimitsu et al., 2025)	CVPR'25	0.39	6.36	1.04	0.91	10.69	1.97	3.56	2.12
	CEDFlow++ (Zuo et al., 2025)	IJCV'25	-	-	1.37	-	-	2.40	4.78	-
	WAFT (Wang & Deng, 2025)	Arxiv'25	-	-	1.09	-	-	2.34	3.42	2.04
Multi-frame	MFCFlow (Chen et al., 2023)	WACV'23	0.65	8.34	1.49	1.33	12.81	2.58	5.00	-
	TransFlow (Lu et al., 2023)	CVPR'23	0.36	6.77	1.06	0.99	10.96	2.08	4.32	-
	SplatFlow (Wang et al., 2024a)	IJCV'24	0.51	6.06	1.12	1.06	10.29	2.07	4.61	2.96
	StreamFlow (Sun et al., 2024)	NeurIPS'24	0.38	6.42	1.04	0.82	10.44	1.87	4.24	2.45
	MemFlow (Dong & Fu, 2024)	CVPR'24	0.43	6.09	1.05	0.93	9.93	1.91	4.10	2.56
	MEMFOF (Bargatin et al., 2025)	ICCV'25	0.40	**5.59**	**0.96**	0.88	10.30	1.91	2.94	1.97
	ARFlow (Ours)	—	0.39	5.64	**0.96**	**0.81**	**9.79**	**1.78**	**2.85**	**1.91**

loss function to stabilize training and guide the learning of $\mathrm{Trans}^{(2)}$ and $\mathrm{Trans}^{(4)}$. From the final token of $\mathrm{Trans}^{(f)}$, we additionally predict a learnable weighting parameter $w_{t,t+1} = \phi_f(\mathbf{Feat}^{(4)}_{\text{fuse}})$. Finally, we re-weight the output from the GRU refinement by incorporating multi-stride forecasted flows by:

$$F_{t,t+1} = w_{t,t+1} f^K_{t,t+1} + (1 - w_{t,t+1}) f_{\text{fuse}}. \tag{8}$$

The weighted optical flow estimation $F_{t,t+1}$ is the final output, which is also leveraged to update the memory bank to forecast the next frame pairs. The final flow estimation $F_{t,t+1}$ are convexly upsampled to the input resolution as in RAFT (Teed & Deng, 2020).

3.4 Loss Functions

Following SEA-RAFT (Wang et al., 2024b), we utilize a mixture-of-Laplace (MoL) loss and apply RAFT-style deep supervision across iterations. Given T frames and K refinement steps, the training loss is

$$\mathcal{L} = \frac{1}{T} \sum_{t=1}^{T} \sum_{k=0}^{K} \gamma^{K-k} \mathcal{L}^{t,k}_{\text{MoL}}, \tag{9}$$

where $\mathcal{L}^{t,k}_{\text{MoL}}$ denotes the MoL loss for frame t at refinement k. Following (Bargatin et al., 2025), we set $\gamma = 0.85$ to emphasize later refinements. Parameterization and mixture details are provided in the supplementary. In addition to K refined flows $f^k_{t,t+1}$, we also apply the same MoL objective to all intermediate flows, including $f_{t,t+1}$, $f^{(2)}_{t,t+1}$, $f^{(4)}_{t,t+1}$, f_{fuse}, and $F_{t,t+1}$.

4 Experiments

4.1 Experimental Settings

Evaluation Datasets and Metrics. We evaluate on three standard optical-flow benchmarks: Spring (Mehl et al., 2023b) (modern high-resolution video), MPI-Sintel (Butler et al., 2012) (synthetic scenes with complex motion), and KITTI-2015 (Menze & Geiger, 2015) (autonomous driving). We report endpoint error (EPE), 1-pixel error rate (1px), Fl (KITTI-15), and WAUC as comparison metrics. The detailed definitions are described in the appendix.

Figure 4: Qualitative comparison on Sintel test set. Compared with previous methods, our ARFlow can predict sharper motion boundaries as highlighted in the circle. Please zoom in for details.

Figure 5: Qualitative comparison on KITTI test set. Compared with previous methods, our ARFlow can distinguish occluded areas as highlighted in the circle. Please zoom in for details.

Network Architectures. For image feature extraction, we use a ResNet–FPN backbone He et al. (2016) (ResNet-34, dim$=512$) shared by the context network (cnet) and feature network (fnet). cnet takes concatenated RGB frames to produce $1/16$-resolution features and the initial hidden state, while fnet extracts per-frame features for subsequent feature matching. On top of these encoders, we adopt a standard RAFT/GMA-style backbone (Jiang et al., 2021) with a 4-stage correlation pyramid (radius=4), a GMAUpdateBlock (num_blocks$=2$, iters$=6$ at $1/16$ resolution), and a learned convex upsampler for GRU-based Iterative Refinement. For the Temporal Transformer, we first encode the optical flow and its uncertainty at each time step using 2D convolutions, transforming the input $(B, T, 6, H, W)$ into features (B, T, C, H, W). We then rearrange them as: $(B, T, C, H, W) \rightarrow (BHW, T, C)$, and apply standard multi-head self-attention along the temporal dimension. Moreover, we adopt multi-scale hierarchical Temporal Transformers (downsampled by the strides=1, 2, 4 over time) and fuse these sequences with another Temporal Transformer in the Auto-regressive Multi-Stride Flow Refinement module.

Pretraining and Fine-Tuning for Benchmark Submissions. We first pretrain on TartanAir (Wang et al., 2020) for 225k steps with a crop size of 480×960, batch size of 64, and a learning rate of 1.4×10^{-4}, which requires about 13.1 GB of GPU memory. This model is then used to initialize training on FlyingThings3D (Mayer et al., 2016) for 120k steps with a larger crop size of 864×1920, batch size 32, and learning rate 7×10^{-5} (18.5 GB). Next, we extend the training to the combined T+S+K+H (FlyingThings (Mayer et al., 2016), Sintel (train) (Butler et al., 2012), KITTI-15 (train) (Geiger et al., 2013), and HD1K (Kondermann et al., 2016)) set for 225k steps under the same settings.

For benchmark-specific adaptation, we perform lightweight fine-tuning. On Sintel, we train 12.5k steps with 872×1920 crops, batch size 8, and learning rate 3×10^{-5}, requiring 23.8 GB of memory. On KITTI-15, we fine-tune 2.5k steps at 750×1920, batch size 32, and learning rate 3×10^{-5}, requiring 20.8 GB of memory. On Spring (Mehl et al., 2023b), we run 60k steps with full-resolution 1080×1920 crops, batch size 8, and learning rate 4.8×10^{-5}, requiring 29.4 GB of memory. We adopt MEMFOF (Bargatin et al., 2025) as the network architecture. By default, the temporal length of the memory bank is $T = 6$, and the GRU refinement performs $K = 6$ iterations. The detailed network implementation is provided in the supplementary code.

Settings for Zero-Shot Evaluation. For zero-shot evaluation, following MemFlow (Dong & Fu, 2024), we first pre-train the networks in the 2-frame setting on FlyingChairs (60k iterations) and FlyingThings3D (150k iterations). We then enable temporal modeling and continue training on FlyingThings3D for an additional 120k iterations.

4.2 Benchmark Results

Benchmark Results on Sintel and KITTI-15. Table 1 reports results on the two widely-used benchmarks. **ARFlow** ranks **first** on the official KITTI-15 benchmark (Geiger et al., 2013), achieving the lowest errors on both *All* pixels (**2.85** vs. 2.94 of MEMFOF and 4.10 of MemFlow) and *Non-Occ* pixels (**1.91** vs. 1.97 of MEMFOF and 2.56 of MemFlow). On Sintel (Butler et al., 2012), ARFlow achieves state-of-the-art performance on the *Final* pass (**1.78** vs. 1.87 of StreamFlow and 1.91 of MEMFOF) and ties the best on *Clean* (0.96). These results highlight the advantage of our auto-regressive framework: *(AFI)* provides reliable initialization values from historical estimates, while *(AMFR)* integrates both short- and long-term temporal cues, enabling more accurate

Table 2: **Benchmark results on Spring.** Runtime and maximum GPU memory usage were evaluated using an NVIDIA RTX 3090 GPU. Best results are respectively highlighted as **first**, second. OOM indicates out of memory. * indicates scene flow methods.

	Method	#Frames	Inference Cost (1080p)		Spring (test)			
			Memory, GB	Runtime, ms	1px ↓	EPE ↓	Fl ↓	WAUC ↑
NO FINE-TUNE	Flow1D (Xu et al., 2021)	2	1.34	405	-	-	-	-
	MeFlow (Xu et al., 2023a)	2	1.32	1028	-	-	-	-
	PWC-Net (Sun et al., 2018b)	2	1.41	76	82.265	2.288	4.889	45.670
	FlowNet2 (Ilg et al., 2017b)	2	4.16	167	6.710	1.040	2.823	90.907
	RAFT (Teed & Deng, 2020)	2	7.97	557	6.790	1.476	3.198	90.920
	RAFT3D* (Teed & Deng, 2021)	2	-	-	13.962	2.528	6.889	81.267
	GMA (Jiang et al., 2021)	2	13.26	1185	7.074	0.914	3.079	90.722
	GMFlow (Xu et al., 2022)	2	-	151	10.355	0.945	2.952	82.337
	FlowFormer (Huang et al., 2022)	2	OOM	-	6.510	0.723	2.384	91.679
	RPKNet (Morimitsu et al., 2024)	2	8.49	295	4.809	0.657	1.756	92.638
	Win-Win (Leroy et al., 2024)	2	-	-	5.371	0.475	1.621	92.720
	MS-RAFT+ (Jahedi et al., 2024)	2	-	-	5.724	0.643	2.189	92.888
	MatchAttention (Yan et al., 2025)	2	14.34	755	4.584	0.453	1.505	93.389
	M-Fuse (F)* (Mehl et al., 2023a)	3	-	-	20.374	2.948	8.791	76.550
	VideoFlow-BOF (Shi et al., 2023a)	3	17.74	1648	-	-	-	-
	VideoFlow-MOF (Shi et al., 2023a)	5	OOM	-	-	-	-	-
	MemFlow (Dong & Fu, 2024)	3	8.08	885	5.759	0.627	2.114	92.253
	StreamFlow (Sun et al., 2024)	4	18.97	929	5.215	0.606	1.856	93.253
	MEMFOF (Bargatin et al., 2025)	3	2.09	472	3.600	0.432	1.353	94.481
	ARFlow (Ours)	8	2.10	403	**3.587**	**0.428**	**1.313**	**94.501**
FINE-TUNE	CrocoFlow (Weinzaepfel et al., 2023)	2	2.01	6524	4.565	0.498	1.508	93.660
	SEA-RAFT (S) (Wang et al., 2024b)	2	8.15	205	3.904	0.377	1.389	94.182
	SEA-RAFT (M) (Wang et al., 2024b)	2	8.19	286	3.686	0.363	1.347	94.534
	MemFlow (Dong & Fu, 2024)	3	8.08	885	4.482	0.471	1.416	93.855
	StreamFlow (Sun et al., 2024)	4	18.97	929	4.152	0.467	1.424	94.404
	DPFlow (Morimitsu et al., 2025)	2	10.39	990	3.442	**0.340**	1.280	94.663
	MEMFOF (Bargatin et al., 2025)	3	2.09	472	3.289	0.355	1.238	95.186
	ARFlow (Ours)	8	2.10	403	**3.265**	0.353	**1.212**	**95.283**

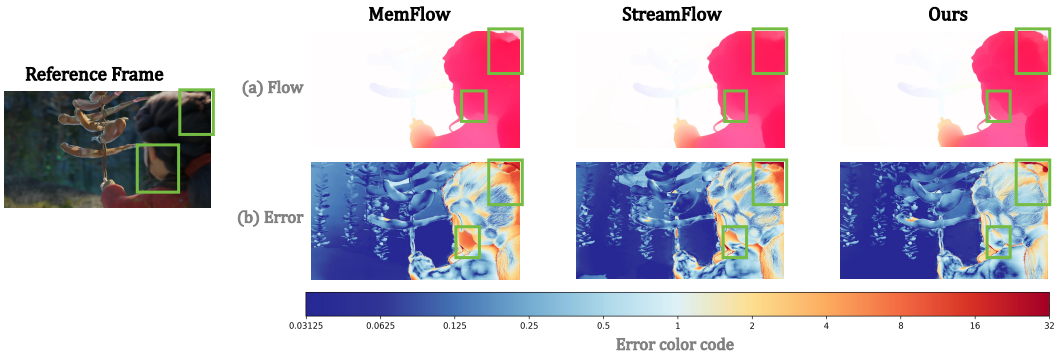

Figure 6: Qualitative comparison on Spring test set. Compared with previous multi-frame methods MemFlow (Dong & Fu, 2024), StreamFlow (Sun et al., 2024), our ARFlow has more accurate flow estimations and lower errors as highlighted in the circle. Please zoom in for details.

and robust predictions. We also visualize the qualitative flow predictions as in Fig. 4 and Fig. 5, respectively. Our ARFlow performs better in terms of sharp boundaries and occluded areas.

Benchmark Results on Spring. Table 2 shows the results on Spring. With full-resolution training (1080p), ARFlow achieves the state-of-the-art performance across all four metrics (1px, EPE, Fl, WAUC), while being highly efficient in both memory (2.1 GB) and runtime. This efficiency stems from avoiding redundant feature extraction and progressively forecasting frame by frame, making ARFlow the only method that combines SOTA accuracy with scalability to long sequences. We also visualize the predicted flow and its corresponding error maps in Fig. 6.

Table 3: **Zero-shot Generalization.** ARFlow achieves the best cross-dataset generalization on KITTI-15 (train).

Method	Sintel		KITTI-15	
	Clean ↓	Final ↓	Fl-EPE ↓	Fl-all ↓
PWC-Net (Sun et al., 2018b)	2.55	3.93	10.40	33.7
FlowNet2 (Ilg et al., 2017a)	2.02	3.14	10.10	30.4
RAFT (Teed & Deng, 2020)	1.43	2.71	5.04	17.4
SKFlow (Sun et al., 2022)	1.22	2.46	4.27	15.5
GMFlowNet (Zhao et al., 2022)	1.14	2.71	4.24	15.4
FlowFormer (Huang et al., 2022)	1.01	2.40	4.09	14.7
SEA-RAFT(L) (Wang et al., 2024b)	1.19	4.11	3.62	12.9
AnyFlow (Jung et al., 2023)	1.10	2.52	3.76	12.4
FlowDiffuser (Luo et al., 2024)	**0.86**	2.19	3.61	11.8
DPFlow (Morimitsu et al., 2025)	1.02	2.26	3.37	11.1
FlowSeek (Poggi & Tosi, 2025)	1.03	2.18	3.31	11.2
WAFT (Wang & Deng, 2025)	1.00	2.15	3.10	10.3
MEMFOF (Bargatin et al., 2025)	1.20	3.91	2.93	9.9
ARFlow (Ours)	0.88	**2.07**	**2.86**	**9.2**

Table 4: **Compatibility evaluation on various baselines.** Consistent with (Wang et al., 2024b; Sun et al., 2022; Morimitsu et al., 2025), all models are trained on the combined Clean+Final (C+T) split and evaluated on the Sintel and KITTI-2015 training sets for a fair comparison. "PG." indicates the performance gain over the baseline.

Method	Sintel (train)			KITTI-2015 (train)		
	Clean ↓	Final ↓	PG.	EPE ↓	F1-all ↓	PG.
SEA-RAFT(L) (Wang et al., 2024b)	1.19	4.11	–	3.62	12.9	–
ARFlow-S	**1.12**	**3.72**	**9.5%** ↑	**3.32**	**11.4**	**11.6%** ↑
DPFlow (Morimitsu et al., 2025)	1.02	2.26	–	3.37	11.1	–
ARFlow-D	**0.97**	**2.14**	**5.3%** ↑	**3.08**	**10.3**	**7.2%** ↑
FlowSeek (Poggi & Tosi, 2025)	1.03	2.18	–	3.31	11.2	–
ARFlow-F	**0.95**	**2.07**	**5.0%** ↑	**3.05**	**10.1**	**9.8%** ↑
WAFT (Wang & Deng, 2025)	1.00	2.15	–	3.10	10.3	–
ARFlow-W	**0.91**	**2.01**	**6.5%** ↑	**2.93**	**9.4**	**8.7%** ↑

4.3 Zero-Shot Generalization

Following common practice from Teed & Deng (2020); Huang et al. (2022); Dong & Fu (2024), we pretrain our model on the FlyingChairs (Dosovitskiy et al., 2015) and FlyingThings3D (Mayer et al., 2016) datasets, and then directly assess its performance on the training splits of Sintel (Butler et al., 2012) and KITTI-15 (Geiger et al., 2013).Table 3 summarizes cross-dataset generalization performance. ARFlow achieves strong transfer performance across Sintel (train) and KITTI-15 (train), consistently outperforming recent baselines. These results demonstrate that our auto-regressive design not only improves benchmark accuracy but also yields robust generalization to unseen datasets.

4.4 Compatibility Evaluation on Other Baselines

As shown in Table 4, ARFlow consistently improves different baselines across Sintel and KITTI-2015. For example, it yields 9.5% and 11.6% gains when integrated with SEA-RAFT, and also achieves 5–10% relative improvements when combined with the SOTA methods DPFlow, FlowSeek, and WAFT. These results indicate that our auto-regressive initialization and multi-stride refinement provide complementary temporal cues, serving as a general plug-in that enhances both transformer- and pyramid-based architectures.

4.5 Ablation Study

Effectiveness of AFI and AMFR. Table 5 (#1) evaluates the influence of the proposed components. Removing the Auto-regressive Flow Initialization (AFI) increases errors notably, e.g., Sintel (Clean/Final) from 0.88/2.07 to 0.95/2.15, and KITTI-2015 EPE rises from 2.86 to 3.05. Similarly, discarding the Auto-regressive Multi-stride Flow Refinement (AMFR) degrades performance (Sintel 0.91/2.13, KITTI-2015 EPE 3.00). These results confirm that both AFI and AMFR are indispensable for accurate and robust estimation.

Stride Design in AMFR. As shown in Table 5 (#2), using only a single stride (1, 2, or 4) yields weaker performance. Combining multi-stride settings achieves the lowest errors (Sintel 0.88/2.07, KITTI-2015 EPE 2.86) compared

Table 5: **Ablation study.** Settings used as default are underlined. All models are trained on C+T for fair comparison.

Method	Sintel (train)		KITTI-2015 (train)	
	Clean↓	Final↓	EPE↓	F1-all↓
#1: ARFlow (AF.) approaches				
AF.-w/o AFI	0.95	2.15	3.05	10.11
AF.-w/o AMFR	0.91	2.13	3.00	9.73
<u>AF.</u>	**0.88**	**2.07**	**2.86**	**9.21**
#2: AMFR Strategy				
Single Stride 1	0.89	2.10	2.89	9.52
Single Stride 2	0.90	2.12	2.93	9.55
Single Stride 4	0.91	2.12	3.00	9.68
<u>Stride $1+2+4$</u>	**0.88**	**2.07**	**2.86**	**9.21**
#3: Temporal Length T				
4	0.91	2.11	2.96	9.43
5	0.90	2.09	2.92	9.41
<u>6</u>	**0.88**	2.07	**2.86**	9.21
7	**0.88**	2.08	2.88	9.19
8	0.89	**2.06**	**2.86**	**9.17**

to any of the single stride settings, demonstrating the benefit of capturing both short- and long-term motions.

Temporal Length. Table 5 (#3) investigates the impact of varying the memory length T. We observe consistent gains when extending from 4 to 6 frames, with the best results at $T = 6$ (KITTI-2015 EPE 2.86, Sintel 0.88/2.07). Further increasing frames shows a marginal change, suggesting a trade-off between accuracy and efficiency.

4.6 Discussion

Attention Weights in Temporal Modeling Transformer. We also visualize the attention weights in our designed auto-regressive transformer module in Fig. 7. We observe that our transformer mainly focuses on dynamic objects and motion boundaries, which can provide an accurate motion prior for the next-frame flow forecasting. This ensures a stable and robust flow initialization, resulting in excellent performance of our ARFlow.

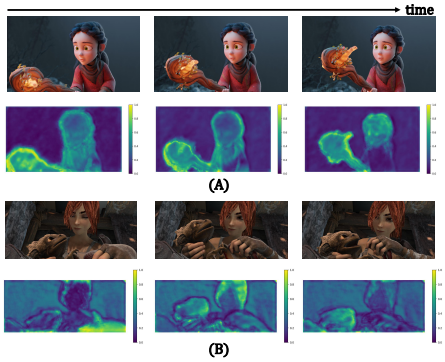

Figure 7: Visualization of attention weights in our temporal modeling transformer.

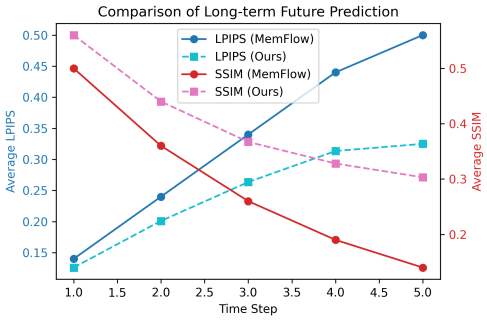

Figure 8: Quantitative comparison of long-term future prediction by optical flow.

Downstream Task: Video Prediction. We evaluate ARFlow against MemFlow under different prediction horizons using LPIPS (lower is better) (Zhang et al., 2018) and SSIM (higher is better) (Wang et al., 2004). As in Fig. 8, when the prediction horizon increases, MemFlow exhibits a rapid degradation in performance, while ARFlow demonstrates a much slower decline, highlighting its stronger temporal modeling and autoregressive prediction capability. Unlike MemFlow, which requires an additional prediction head, ARFlow naturally predicts the next-frame optical flow, leading to more stable and consistent performance over longer horizons. Additional implementation details are provided in the supplementary material.

5 Conclusion

In this paper, we propose a novel multi-frame optical flow estimation pipeline based on auto-regressive transformer models. We formulate the task with the progressive flow estimation frame by frame and introduce an auto-regressive next-frame forecasting strategy to provide accurate and robust initial flow. Then, a refinement module combining both current motion features and multi-stride history forecasting flows is leveraged to generate fine-grained flow estimates and refine the initial predictions. Extensive experiments on standard benchmarks demonstrate that our method achieves state-of-the-art accuracy while maintaining competitive efficiency.

ACKNOWLEDGEMENTS

This work was supported by National Key R&D Program of China (Grant No.2024YFB4708900) and EU HORIZON-CL4-2023-HUMAN-01-CNECT XTREME (Grant No. 101136006). It was also supported in part by the Natural Science Foundation of China under Grant 62225309,U24A20278, 62361166632.

REFERENCES

Vladislav Bargatin, Egor Chistov, Alexander Yakovenko, and Dmitriy Vatolin. Memfof: High-resolution training for memory-efficient multi-frame optical flow estimation. *arXiv preprint arXiv:2506.23151*, 2025.

Michael J Black and Padmanabhan Anandan. A framework for the robust estimation of optical flow. In *1993 (4th) International Conference on Computer Vision*, pp. 231–236. IEEE, 1993.

Andrés Bruhn, Joachim Weickert, and Christoph Schnörr. Lucas/kanade meets horn/schunck: Combining local and global optic flow methods. *International journal of computer vision*, 61(3): 211–231, 2005.

Daniel J Butler, Jonas Wulff, Garrett B Stanley, and Michael J Black. A naturalistic open source movie for optical flow evaluation. In *ECCV*, pp. 611–625. Springer, 2012.

Holger Caesar, Varun Bankiti, Alex H Lang, Sourabh Vora, Venice Erin Liong, Qiang Xu, Anush Krishnan, Yu Pan, Giancarlo Baldan, and Oscar Beijbom. nuscenes: A multimodal dataset for autonomous driving. In *CVPR*, 2020.

Jiewen Chan, Zhenjun Zhao, and Yu-Lun Liu. Adagar: Adaptive gabor representation for dynamic scene reconstruction. *arXiv preprint arXiv:2601.00796*, 2026.

Yonghu Chen, Dongchen Zhu, Wenjun Shi, Guanghui Zhang, Tianyu Zhang, Xiaolin Zhang, and Jiamao Li. Mfcflow: A motion feature compensated multi-frame recurrent network for optical flow estimation. In *Proceedings of the IEEE/CVF Winter conference on applications of computer vision*, pp. 5068–5077, 2023.

Hao Cheng, Mengmeng Liu, and Lin Chen. An end-to-end framework of road user detection, tracking, and prediction from monocular images. In *2023 IEEE 26th International Conference on Intelligent Transportation Systems (ITSC)*, pp. 2178–2185. IEEE, 2023a.

Hao Cheng, Mengmeng Liu, Lin Chen, Hellward Broszio, Monika Sester, and Michael Ying Yang. Gatraj: A graph-and attention-based multi-agent trajectory prediction model. *ISPRS Journal of Photogrammetry and Remote Sensing*, 205:163–175, 2023b.

Andrea Ciamarra, Federico Becattini, Lorenzo Seidenari, and Alberto Del Bimbo. Forecasting future instance segmentation with learned optical flow and warping. In *International Conference on Image Analysis and Processing*, pp. 349–361. Springer, 2022.

Haoge Deng, Ting Pan, Haiwen Diao, Zhengxiong Luo, Yufeng Cui, Huchuan Lu, Shiguang Shan, Yonggang Qi, and Xinlong Wang. Autoregressive video generation without vector quantization. In *The Thirteenth International Conference on Learning Representations*, 2025a. URL `https://openreview.net/forum?id=JE9tCwe3lp`.

Tianchen Deng, Yaohui Chen, Jianfei Yang, Shenghai Yuan, Jiuming Liu, Danwei Wang, and Weidong Chen. Cgs-slam: Compact 3d gaussian splatting for dense visual slam. In *2025 IEEE/RSJ International Conference on Intelligent Robots and Systems (IROS)*, pp. 1606–1613. IEEE, 2025b.

Tianchen Deng, Yue Pan, Shenghai Yuan, Dong Li, Chen Wang, Mingrui Li, Long Chen, Lihua Xie, Danwei Wang, Jingchuan Wang, Javier Civera, Hesheng Wang, and Weidong Chen. What is the best 3d scene representation for robotics? from geometric to foundation models. *arXiv preprint arXiv:2512.03422*, 2025c.

Qiaole Dong and Yanwei Fu. Memflow: Optical flow estimation and prediction with memory. In *Proceedings of the IEEE/CVF Conference on Computer Vision and Pattern Recognition*, pp. 19068–19078, 2024.

Qiaole Dong, Chenjie Cao, and Yanwei Fu. Incremental transformer structure enhanced image inpainting with masking positional encoding. In *Proceedings of the IEEE/CVF Conference on Computer Vision and Pattern Recognition*, pp. 11358–11368, 2022.

Alexey Dosovitskiy, Philipp Fischer, Eddy Ilg, Philip Hausser, Caner Hazirbas, Vladimir Golkov, Patrick Van Der Smagt, Daniel Cremers, and Thomas Brox. Flownet: Learning optical flow with convolutional networks. In *Proceedings of the IEEE international conference on computer vision*, pp. 2758–2766, 2015.

Zhiheng Feng, Jiuming Liu, and Hesheng Wang. Optimizing scene flow with neural rigidity prior. *Robot Learning*, 1(1):1–15, 2024.

Wenhang Ge, Guibao Shen, Jiawei Feng, Luozhou Wang, Hao Lu, Xingye Tian, Xin Tao, and Ying-Cong Chen. Campilot: Improving camera control in video diffusion model with efficient camera reward feedback. *arXiv preprint arXiv:2601.16214*, 2026.

Andreas Geiger, Philip Lenz, Christoph Stiller, and Raquel Urtasun. Vision meets robotics: The kitti dataset. *The International Journal of Robotics Research*, 32(11):1231–1237, 2013.

Kaiming He, Xiangyu Zhang, Shaoqing Ren, and Jian Sun. Deep residual learning for image recognition. In *CVPR*, pp. 770–778, 2016.

Tom Henighan, Jared Kaplan, Mor Katz, Mark Chen, Christopher Hesse, Jacob Jackson, Heewoo Jun, Tom B Brown, Prafulla Dhariwal, Scott Gray, et al. Scaling laws for autoregressive generative modeling. *arXiv preprint arXiv:2010.14701*, 2020.

Roberto Henschel, Levon Khachatryan, Hayk Poghosyan, Daniil Hayrapetyan, Vahram Tadevosyan, Zhangyang Wang, Shant Navasardyan, and Humphrey Shi. Streamingt2v: Consistent, dynamic, and extendable long video generation from text. In *Proceedings of the Computer Vision and Pattern Recognition Conference*, pp. 2568–2577, 2025.

Berthold KP Horn and Brian G Schunck. Determining optical flow. *Artificial intelligence*, 17(1-3): 185–203, 1981.

Xun Huang, Zhengqi Li, Guande He, Mingyuan Zhou, and Eli Shechtman. Self forcing: Bridging the train-test gap in autoregressive video diffusion. In *The Thirty-ninth Annual Conference on Neural Information Processing Systems*, 2025. URL https://openreview.net/forum?id=mSiN7i0BYH.

Zhaoyang Huang, Xiaoyu Shi, Chao Zhang, Qiang Wang, Ka Chun Cheung, Hongwei Qin, Jifeng Dai, and Hongsheng Li. Flowformer: A transformer architecture for optical flow. In *ECCV*, pp. 668–685. Springer, 2022.

Tak-Wai Hui, Xiaoou Tang, and Chen Change Loy. Liteflownet: A lightweight convolutional neural network for optical flow estimation. In *Proceedings of the IEEE conference on computer vision and pattern recognition*, pp. 8981–8989, 2018.

Tak-Wai Hui, Xiaoou Tang, and Chen Change Loy. A lightweight optical flow cnn—revisiting data fidelity and regularization. *IEEE transactions on pattern analysis and machine intelligence*, 43 (8):2555–2569, 2020.

Junhwa Hur and Stefan Roth. Self-supervised multi-frame monocular scene flow. In *Proceedings of the IEEE/CVF Conference on Computer Vision and Pattern Recognition*, pp. 2684–2694, 2021.

Eddy Ilg, Nikolaus Mayer, Tonmoy Saikia, Margret Keuper, Alexey Dosovitskiy, and Thomas Brox. Flownet 2.0: Evolution of optical flow estimation with deep networks. In *Proceedings of the IEEE conference on computer vision and pattern recognition*, pp. 2462–2470, 2017a.

Eddy Ilg, Nikolaus Mayer, Tonmoy Saikia, Margret Keuper, Alexey Dosovitskiy, and Thomas Brox. Flownet 2.0: Evolution of optical flow estimation with deep networks. In *CVPR*, pp. 2462–2470, 2017b.

Azin Jahedi, Maximilian Luz, Marc Rivinius, Lukas Mehl, and Andrés Bruhn. Ms-raft+: High resolution multi-scale raft. *International Journal of Computer Vision*, pp. 1–22, 2023.

Azin Jahedi, Maximilian Luz, Marc Rivinius, Lukas Mehl, and Andrés Bruhn. Ms-raft+: high resolution multi-scale raft. *International Journal of Computer Vision*, 132(5):1835–1856, 2024.

Chaokang Jiang, Guangming Wang, Jiuming Liu, Hesheng Wang, Zhuang Ma, Zhenqiang Liu, Zhujin Liang, Yi Shan, and Dalong Du. 3dsflabelling: Boosting 3d scene flow estimation by pseudo auto-labelling. In *Proceedings of the IEEE/CVF Conference on Computer Vision and Pattern Recognition*, pp. 15173–15183, 2024.

Shihao Jiang, Dylan Campbell, Yao Lu, Hongdong Li, and Richard Hartley. Learning to estimate hidden motions with global motion aggregation. In *Proceedings of the IEEE/CVF international conference on computer vision*, pp. 9772–9781, 2021.

Hyunyoung Jung, Zhuo Hui, Lei Luo, Haitao Yang, Feng Liu, Sungjoo Yoo, Rakesh Ranjan, and Denis Demandolx. Anyflow: Arbitrary scale optical flow with implicit neural representation. In *Proceedings of the IEEE/CVF Conference on Computer Vision and Pattern Recognition*, pp. 5455–5465, 2023.

Daniel Kondermann, Rahul Nair, Katrin Honauer, Karsten Krispin, Jonas Andrulis, Alexander Brock, Burkhard Gussefeld, Mohsen Rahimimoghaddam, Sabine Hofmann, Claus Brenner, et al. The hci benchmark suite: Stereo and flow ground truth with uncertainties for urban autonomous driving. In *Proceedings of the IEEE Conference on Computer Vision and Pattern Recognition Workshops*, pp. 19–28, 2016.

Vincent Leroy, Jerome Revaud, Thomas Lucas, and Philippe Weinzaepfel. Win-win: Training high-resolution vision transformers from two windows. In *The Twelfth International Conference on Learning Representations*, 2024. URL https://openreview.net/forum?id=N23A4ybMJr.

Haoang Li, Ji Zhao, Jean-Charles Bazin, Pyojin Kim, Kyungdon Joo, Zhenjun Zhao, and Yun-Hui Liu. Hong kong world: Leveraging structural regularity for line-based slam. *IEEE Transactions on Pattern Analysis and Machine Intelligence*, 45(11):13035–13053, 2023.

Zhen Li, Cheng-Ze Lu, Jianhua Qin, Chun-Le Guo, and Ming-Ming Cheng. Towards an end-to-end framework for flow-guided video inpainting. In *Proceedings of the IEEE/CVF conference on computer vision and pattern recognition*, pp. 17562–17571, 2022.

Feng Liang, Bichen Wu, Jialiang Wang, Licheng Yu, Kunpeng Li, Yinan Zhao, Ishan Misra, Jia-Bin Huang, Peizhao Zhang, Peter Vajda, et al. Flowvid: Taming imperfect optical flows for consistent video-to-video synthesis. In *Proceedings of the IEEE/CVF Conference on Computer Vision and Pattern Recognition*, pp. 8207–8216, 2024a.

Jingyun Liang, Yuchen Fan, Kai Zhang, Radu Timofte, Luc Van Gool, and Rakesh Ranjan. Movideo: Motion-aware video generation with diffusion model. In *European Conference on Computer Vision*, pp. 56–74. Springer, 2024b.

Haisong Liu, Tao Lu, Yihui Xu, Jia Liu, Wenjie Li, and Lijun Chen. Camliflow: bidirectional camera-lidar fusion for joint optical flow and scene flow estimation. In *Proceedings of the IEEE/CVF conference on computer vision and pattern recognition*, pp. 5791–5801, 2022.

Haisong Liu, Tao Lu, Yihui Xu, Jia Liu, and Limin Wang. Learning optical flow and scene flow with bidirectional camera-lidar fusion. *IEEE Transactions on Pattern Analysis and Machine Intelligence*, 46(4):2378–2395, 2023a.

Jinlai Liu, Jian Han, Bin Yan, Wuhui, Fengda Zhu, Xing Wang, Yi Jiang, BINGYUE PENG, and Zehuan Yuan. Infinitystar: Unified spacetime autoregressive modeling for visual generation. In *The Thirty-ninth Annual Conference on Neural Information Processing Systems*, 2025a. URL https://openreview.net/forum?id=JcEqp4aPmb.

Jiuming Liu, Guangming Wang, Chaokang Jiang, Zhe Liu, and Hesheng Wang. Translo: A window-based masked point transformer framework for large-scale lidar odometry. In *Proceedings of the AAAI Conference on Artificial Intelligence*, volume 37, pp. 1683–1691, 2023b.

Jiuming Liu, Guangming Wang, Zhe Liu, Chaokang Jiang, Marc Pollefeys, and Hesheng Wang. Regformer: An efficient projection-aware transformer network for large-scale point cloud registration. In *Proceedings of the IEEE/CVF International Conference on Computer Vision*, pp. 8451–8460, 2023c.

Jiuming Liu, Guangming Wang, Weicai Ye, Chaokang Jiang, Jinru Han, Zhe Liu, Guofeng Zhang, Dalong Du, and Hesheng Wang. Difflow3d: Toward robust uncertainty-aware scene flow estimation with iterative diffusion-based refinement. In *Proceedings of the IEEE/CVF Conference on Computer Vision and Pattern Recognition*, pp. 15109–15119, 2024a.

Jiuming Liu, Ruiji Yu, Yian Wang, Yu Zheng, Tianchen Deng, Weicai Ye, and Hesheng Wang. Point mamba: A novel point cloud backbone based on state space model with octree-based ordering strategy. *arXiv preprint arXiv:2403.06467*, 2024b.

Jiuming Liu, Dong Zhuo, Zhiheng Feng, Siting Zhu, Chensheng Peng, Zhe Liu, and Hesheng Wang. Dvlo: Deep visual-lidar odometry with local-to-global feature fusion and bi-directional structure alignment. In *European Conference on Computer Vision*, pp. 475–493. Springer, 2024c.

Jiuming Liu, Jinru Han, Lihao Liu, Angelica I Aviles-Rivero, Chaokang Jiang, Zhe Liu, and Hesheng Wang. Mamba4d: Efficient 4d point cloud video understanding with disentangled spatial-temporal state space models. In *Proceedings of the Computer Vision and Pattern Recognition Conference*, pp. 17626–17636, 2025b.

Jiuming Liu, Zheng Huang, Mengmeng Liu, Tianchen Deng, Francesco Nex, Hao Cheng, and Hesheng Wang. Topolidm: Topology-aware lidar diffusion models for interpretable and realistic lidar point cloud generation. In *2025 IEEE/RSJ International Conference on Intelligent Robots and Systems (IROS)*, pp. 8180–8186. IEEE, 2025c.

Jiuming Liu, Weicai Ye, Guangming Wang, Chaokang Jiang, Lei Pan, Jinru Han, Zhe Liu, Guofeng Zhang, and Hesheng Wang. Difflow3d: Hierarchical diffusion models for uncertainty-aware 3d scene flow estimation. *IEEE transactions on pattern analysis and machine intelligence*, 2025d.

Mengmeng Liu, Hao Cheng, and Michael Ying Yang. Tracing the influence of predecessors on trajectory prediction. In *Proceedings of the IEEE/CVF International Conference on Computer Vision*, pp. 3253–3263, 2023d.

Mengmeng Liu, Hao Cheng, Lin Chen, Hellward Broszio, Jiangtao Li, Runjiang Zhao, Monika Sester, and Michael Ying Yang. Laformer: Trajectory prediction for autonomous driving with lane-aware scene constraints. In *Proceedings of the IEEE/CVF conference on computer vision and pattern recognition*, pp. 2039–2049, 2024d.

Mengmeng Liu, Jiuming Liu, Yunpeng Zhang, Jiangtao Li, Michael Ying Yang, Francesco Nex, and Hao Cheng. 4dstr: Advancing generative 4d gaussians with spatial-temporal rectification for high-quality and consistent 4d generation. *arXiv preprint arXiv:2511.07241*, 2025e.

Mengmeng Liu, Michael Ying Yang, Jiuming Liu, Yunpeng Zhang, Jiangtao Li, Sander Oude Elberink, George Vosselman, and Hao Cheng. Dvlo4d: Deep visual-lidar odometry with sparse spatial-temporal fusion. In *2025 IEEE International Conference on Robotics and Automation (ICRA)*, pp. 9740–9747. IEEE, 2025f.

Pengpeng Liu, Michael Lyu, Irwin King, and Jia Xu. Selflow: Self-supervised learning of optical flow. In *Proceedings of the IEEE/CVF conference on computer vision and pattern recognition*, pp. 4571–4580, 2019.

Hao LU, Tianshuo Xu, Wenzhao Zheng, Yunpeng Zhang, Wei Zhan, Dalong Du, Masayoshi Tomizuka, Kurt Keutzer, and Ying-Cong Chen. Drivingrecon: Large 4d gaussian reconstruction model for autonomous driving. In *The Thirty-ninth Annual Conference on Neural Information Processing Systems*, 2025. URL https://openreview.net/forum?id=HF5A73jmxq.

Yawen Lu, Qifan Wang, Siqi Ma, Tong Geng, Yingjie Victor Chen, Huaijin Chen, and Dongfang Liu. Transflow: Transformer as flow learner. In *Proceedings of the IEEE/CVF Conference on Computer Vision and Pattern Recognition*, pp. 18063–18073, 2023.

Ao Luo, Fan Yang, Xin Li, Lang Nie, Chunyu Lin, Haoqiang Fan, and Shuaicheng Liu. Gaflow: Incorporating gaussian attention into optical flow. In *Proceedings of the IEEE/CVF International Conference on Computer Vision*, pp. 9642–9651, 2023.

Ao Luo, Xin Li, Fan Yang, Jiangyu Liu, Haoqiang Fan, and Shuaicheng Liu. Flowdiffuser: Advancing optical flow estimation with diffusion models. In *Proceedings of the IEEE/CVF Conference on Computer Vision and Pattern Recognition*, pp. 19167–19176, 2024.

Nikolaus Mayer, Eddy Ilg, Philip Hausser, Philipp Fischer, Daniel Cremers, Alexey Dosovitskiy, and Thomas Brox. A large dataset to train convolutional networks for disparity, optical flow, and scene flow estimation. In *Proceedings of the IEEE conference on computer vision and pattern recognition*, pp. 4040–4048, 2016.

Lukas Mehl, Azin Jahedi, Jenny Schmalfuss, and Andrés Bruhn. M-fuse: Multi-frame fusion for scene flow estimation. In *Proceedings of the IEEE/CVF Winter Conference on Applications of Computer Vision*, pp. 2020–2029, 2023a.

Lukas Mehl, Jenny Schmalfuss, Azin Jahedi, Yaroslava Nalivayko, and Andrés Bruhn. Spring: A high-resolution high-detail dataset and benchmark for scene flow, optical flow and stereo. In *CVPR*, pp. 4981–4991, 2023b.

Moritz Menze and Andreas Geiger. Object scene flow for autonomous vehicles. In *Proceedings of the IEEE conference on computer vision and pattern recognition*, pp. 3061–3070, 2015.

Henrique Morimitsu, Xiaobin Zhu, Xiangyang Ji, and Xu-Cheng Yin. Recurrent partial kernel network for efficient optical flow estimation. 2024.

Henrique Morimitsu, Xiaobin Zhu, Roberto M Cesar, Xiangyang Ji, and Xu-Cheng Yin. Dpflow: Adaptive optical flow estimation with a dual-pyramid framework. In *Proceedings of the Computer Vision and Pattern Recognition Conference*, pp. 17810–17820, 2025.

Simon Niklaus and Feng Liu. Softmax splatting for video frame interpolation. In *IEEE Conference on Computer Vision and Pattern Recognition*, 2020.

Matteo Poggi and Fabio Tosi. Flowseek: Optical flow made easier with depth foundation models and motion bases, 2025. URL `https://arxiv.org/abs/2509.05297`.

René Ranftl, Alexey Bochkovskiy, and Vladlen Koltun. Vision transformers for dense prediction. In *Proceedings of the IEEE/CVF international conference on computer vision*, pp. 12179–12188, 2021.

Anurag Ranjan and Michael J Black. Optical flow estimation using a spatial pyramid network. In *CVPR*, pp. 4161–4170, 2017.

Stephan R Richter, Zeeshan Hayder, and Vladlen Koltun. Playing for benchmarks. In *ICCV*, pp. 2213–2222, 2017.

Saurabh Saxena, Charles Herrmann, Junhwa Hur, Abhishek Kar, Mohammad Norouzi, Deqing Sun, and David J Fleet. The surprising effectiveness of diffusion models for optical flow and monocular depth estimation. *Advances in Neural Information Processing Systems*, 36:39443–39469, 2023.

Jiayao Shan, Sifan Zhou, Zheng Fang, and Yubo Cui. Ptt: Point-track-transformer module for 3d single object tracking in point clouds. In *2021 IEEE/RSJ International Conference on Intelligent Robots and Systems (IROS)*, pp. 1310–1316. IEEE, 2021.

Xiaoyu Shi, Zhaoyang Huang, Weikang Bian, Dasong Li, Manyuan Zhang, Ka Chun Cheung, Simon See, Hongwei Qin, Jifeng Dai, and Hongsheng Li. Videoflow: Exploiting temporal cues for multi-frame optical flow estimation. In *ICCV*, pp. 12469–12480, 2023a.

Xiaoyu Shi, Zhaoyang Huang, Dasong Li, Manyuan Zhang, Ka Chun Cheung, Simon See, Hongwei Qin, Jifeng Dai, and Hongsheng Li. Flowformer++: Masked cost volume autoencoding for pretraining optical flow estimation. In *CVPR*, pp. 1599–1610, 2023b.

Xiuchao Sui, Shaohua Li, Xue Geng, Yan Wu, Xinxing Xu, Yong Liu, Rick Goh, and Hongyuan Zhu. Craft: Cross-attentional flow transformer for robust optical flow. In *Proceedings of the IEEE/CVF conference on Computer Vision and Pattern Recognition*, pp. 17602–17611, 2022.

Deqing Sun, Xiaodong Yang, Ming-Yu Liu, and Jan Kautz. Pwc-net: Cnns for optical flow using pyramid, warping, and cost volume. In *Proceedings of the IEEE/CVF Conference on Computer Vision and Pattern Recognition*, 2018a.

Deqing Sun, Xiaodong Yang, Ming-Yu Liu, and Jan Kautz. Pwc-net: Cnns for optical flow using pyramid, warping, and cost volume. In *CVPR*, pp. 8934–8943, 2018b.

Pei Sun, Henrik Kretzschmar, Xerxes Dotiwalla, Aurelien Chouard, Vijaysai Patnaik, Paul Tsui, James Guo, Yin Zhou, Yuning Chai, Benjamin Caine, et al. Scalability in perception for autonomous driving: Waymo open dataset. In *Proceedings of the IEEE/CVF conference on computer vision and pattern recognition*, pp. 2446–2454, 2020.

Shangkun Sun, Yuanqi Chen, Yu Zhu, Guodong Guo, and Ge Li. Skflow: Learning optical flow with super kernels. *Advances in Neural Information Processing Systems*, 35:11313–11326, 2022.

Shangkun Sun, Jiaming Liu, Huaxia Li, Guoqing Liu, Thomas Li, and Wei Gao. Streamflow: streamlined multi-frame optical flow estimation for video sequences. *Advances in neural information processing systems*, 37:9205–9228, 2024.

Jiaqi Tang, Hao Lu, Ruizheng Wu, Xiaogang Xu, Ke Ma, Cheng Fang, Bin Guo, Jiangbo Lu, Qifeng Chen, and Yingcong Chen. Hawk: Learning to understand open-world video anomalies. *Advances in Neural Information Processing Systems*, 37:139751–139785, 2024.

Meituan LongCat Team, Xunliang Cai, Qilong Huang, Zhuoliang Kang, Hongyu Li, Shijun Liang, Liya Ma, Siyu Ren, Xiaoming Wei, Rixu Xie, et al. Longcat-video technical report. *arXiv preprint arXiv:2510.22200*, 2025.

Zachary Teed and Jia Deng. Raft: Recurrent all-pairs field transforms for optical flow. In *Computer Vision–ECCV 2020: 16th European Conference, Glasgow, UK, August 23–28, 2020, Proceedings, Part II 16*, pp. 402–419. Springer, 2020.

Zachary Teed and Jia Deng. Raft-3d: Scene flow using rigid-motion embeddings. In *Proceedings of the IEEE/CVF conference on computer vision and pattern recognition*, pp. 8375–8384, 2021.

Team Wan, Ang Wang, Baole Ai, Bin Wen, Chaojie Mao, Chen-Wei Xie, Di Chen, Feiwu Yu, Haiming Zhao, Jianxiao Yang, et al. Wan: Open and advanced large-scale video generative models. *arXiv preprint arXiv:2503.20314*, 2025.

Bo Wang, Yifan Zhang, Jian Li, Yang Yu, Zhenping Sun, Li Liu, and Dewen Hu. Splatflow: Learning multi-frame optical flow via splatting. *International Journal of Computer Vision*, 132(8):3023–3045, 2024a.

Wenshan Wang, Delong Zhu, Xiangwei Wang, Yaoyu Hu, Yuheng Qiu, Chen Wang, Yafei Hu, Ashish Kapoor, and Sebastian Scherer. Tartanair: A dataset to push the limits of visual slam. In *2020 IEEE/RSJ International Conference on Intelligent Robots and Systems (IROS)*, pp. 4909–4916. IEEE, 2020.

Yihan Wang and Jia Deng. Waft: Warping-alone field transforms for optical flow. *arXiv preprint arXiv:2506.21526*, 2025.

Yihan Wang, Lahav Lipson, and Jia Deng. Sea-raft: Simple, efficient, accurate raft for optical flow. In *European Conference on Computer Vision*, pp. 36–54. Springer, 2024b.

Zhou Wang, Alan C Bovik, Hamid R Sheikh, and Eero P Simoncelli. Image quality assessment: from error visibility to structural similarity. *IEEE transactions on image processing*, 13(4):600–612, 2004.

Philippe Weinzaepfel, Thomas Lucas, Vincent Leroy, Yohann Cabon, Vaibhav Arora, Romain Brégier, Gabriela Csurka, Leonid Antsfeld, Boris Chidlovskii, and Jérôme Revaud. Croco v2: Improved cross-view completion pre-training for stereo matching and optical flow. In *Proceedings of the IEEE/CVF International Conference on Computer Vision*, pp. 17969–17980, 2023.

Desai Xie, Zhan Xu, Yicong Hong, Hao Tan, Difan Liu, Feng Liu, Arie Kaufman, and Yang Zhou. Progressive autoregressive video diffusion models. In *Proceedings of the Computer Vision and Pattern Recognition Conference*, pp. 6322–6332, 2025.

Gangwei Xu, Shujun Chen, Hao Jia, Miaojie Feng, and Xin Yang. Memory-efficient optical flow via radius-distribution orthogonal cost volume. *arXiv preprint arXiv:2312.03790*, 2023a.

Haofei Xu, Jiaolong Yang, Jianfei Cai, Juyong Zhang, and Xin Tong. High-resolution optical flow from 1d attention and correlation. In *ICCV*, pp. 10498–10507, 2021.

Haofei Xu, Jing Zhang, Jianfei Cai, Hamid Rezatofighi, and Dacheng Tao. Gmflow: Learning optical flow via global matching. In *CVPR*, pp. 8121–8130, 2022.

Haofei Xu, Jing Zhang, Jianfei Cai, Hamid Rezatofighi, Fisher Yu, Dacheng Tao, and Andreas Geiger. Unifying flow, stereo and depth estimation. *IEEE Transactions on Pattern Analysis and Machine Intelligence*, 2023b.

Rui Xu, Xiaoxiao Li, Bolei Zhou, and Chen Change Loy. Deep flow-guided video inpainting. In *Proceedings of the IEEE/CVF Conference on Computer Vision and Pattern Recognition*, pp. 3723–3732, 2019.

Tianshuo Xu, Zhifei Chen, Leyi Wu, Hao Lu, Yuying Chen, Lihui Jiang, Bingbing Liu, and Yingcong Chen. Motion dreamer: Boundary conditional motion reasoning for physically coherent video generation. *arXiv preprint arXiv:2412.00547*, 2024.

Tingman Yan, Tao Liu, Xilian Yang, Qunfei Zhao, and Zeyang Xia. Matchattention: Matching the relative positions for high-resolution cross-view matching. *arXiv preprint arXiv:2510.14260*, 2025.

Gengshan Yang and Deva Ramanan. Volumetric correspondence networks for optical flow. *Advances in neural information processing systems*, 32:794–805, 2019.

Tianwei Yin, Qiang Zhang, Richard Zhang, William T Freeman, Fredo Durand, Eli Shechtman, and Xun Huang. From slow bidirectional to fast autoregressive video diffusion models. In *Proceedings of the Computer Vision and Pattern Recognition Conference*, pp. 22963–22974, 2025.

Fangao Zeng, Bin Dong, Yuang Zhang, Tiancai Wang, Xiangyu Zhang, and Yichen Wei. Motr: End-to-end multiple-object tracking with transformer. In *ECCV*, 2022.

Shangjin Zhai, Zhichao Ye, Jialin Liu, Weijian Xie, Jiaqi Hu, Zhen Peng, Hua Xue, Danpeng Chen, Xiaomeng Wang, Lei Yang, et al. Stargen: A spatiotemporal autoregression framework with video diffusion model for scalable and controllable scene generation. In *Proceedings of the Computer Vision and Pattern Recognition Conference*, pp. 26822–26833, 2025.

Feihu Zhang, Oliver J Woodford, Victor Adrian Prisacariu, and Philip HS Torr. Separable flow: Learning motion cost volumes for optical flow estimation. In *Proceedings of the IEEE/CVF International Conference on Computer Vision*, pp. 10807–10817, 2021.

Qingwen Zhang, Yi Yang, Peizheng Li, Olov Andersson, and Patric Jensfelt. Seflow: A self-supervised scene flow method in autonomous driving. In *European Conference on Computer Vision*, pp. 353–369. Springer, 2024.

Qingwen Zhang, Xiaomeng Zhu, Yushan Zhang, Yixi Cai, Olov Andersson, and Patric Jensfelt. Deltaflow: An efficient multi-frame scene flow estimation method. In *The Thirty-ninth Annual Conference on Neural Information Processing Systems*, 2025. URL https://openreview.net/forum?id=T9qNDtvAJX.

Richard Zhang, Phillip Isola, Alexei A Efros, Eli Shechtman, and Oliver Wang. The unreasonable effectiveness of deep features as a perceptual metric. In *Proceedings of the IEEE conference on computer vision and pattern recognition*, pp. 586–595, 2018.

Shiyu Zhao, Long Zhao, Zhixing Zhang, Enyu Zhou, and Dimitris Metaxas. Global matching with overlapping attention for optical flow estimation. In *Proceedings of the IEEE/CVF Conference on Computer Vision and Pattern Recognition*, pp. 17592–17601, 2022.

Yang Zhao, Gangwei Xu, and Gang Wu. Hybrid cost volume for memory-efficient optical flow. In *Proceedings of the 32nd ACM International Conference on Multimedia*, pp. 8740–8749, 2024.

Deyu Zhou, Quan Sun, Yuang Peng, Kun Yan, Runpei Dong, Duomin Wang, Zheng Ge, Nan Duan, and Xiangyu Zhang. Taming teacher forcing for masked autoregressive video generation. In *Proceedings of the Computer Vision and Pattern Recognition Conference*, pp. 7374–7384, 2025.

Shili Zhou, Ruian He, Weimin Tan, and Bo Yan. Samflow: Eliminating any fragmentation in optical flow with segment anything model. In *Proceedings of the AAAI Conference on Artificial Intelligence*, volume 38, pp. 7695–7703, 2024.

Siting Zhu, Guangming Wang, Hermann Blum, Jiuming Liu, Liang Song, Marc Pollefeys, and Hesheng Wang. Sni-slam: Semantic neural implicit slam. In *Proceedings of the IEEE/CVF Conference on Computer Vision and Pattern Recognition*, pp. 21167–21177, 2024.

Fengyuan Zuo, Haiyan Jin, Zhaolin Xiao, Haonan Su, and Meng Zhang. Cedflow++: Latent contour enhancement for dark optical flow estimation. *International Journal of Computer Vision*, pp. 1–20, 2025.

APPENDIX

A OVERVIEW

The supplementary materials are structured as follows:

- We give more detailed illustrations about the metrics, loss functions, settings in video prediction, and clip-wise training strategy in Section B;
- More experimental results are provided in Section C.
- Qualitative results on KITTI, Waymo, and NuScenes are presented in Section D;
- Screenshots for benchmark results on KITTI, Sintel, and Spring are shown in Section E;
- Section F discloses the limited and strictly assistive usage of a large language model (LLM) during manuscript polishing.
- A video demo of both synthetic and real-world driving scenes is appended to the supplementary materials, and the detailed network implementation is also provided in the supplementary code.

B IMPLEMENTATION DETAILS

B.1 DEFINITION OF METRICS

We provide more formal definitions of metrics used in the main text.

- EPE is the average per-pixel Euclidean distance between the predicted flow and the reference flow over all valid pixels.
- The 1px rate is the fraction of valid pixels whose flow error exceeds one pixel.
- The Fl score (KITTI-2015) is the percentage of pixels whose error is larger than three pixels and also greater than five percent of the ground-truth magnitude.
- WAUC summarizes performance by integrating the inlier rate over error thresholds from zero to five pixels, with larger weights near zero; a precise definition appears in the supplementary material. For optical flow, the weighted area under the inlier-rate curve (WAUC), introduced with VIPER (Richter et al., 2017), aggregates the inlier percentage over error thresholds.

Let $f(\tau) \in [0, 100]$ denote the percentage of pixels whose endpoint error is at most τ pixels. With a weight that emphasizes small thresholds, the metric is

$$\text{WAUC} \;=\; \frac{2}{5} \int_0^5 f(\tau)\, \frac{5-\tau}{5}\, d\tau, \tag{10}$$

yielding a score between 0 (worst) and 100 (best).

B.2 MIXTURE-OF-LAPLACE LOSS

Following SEA-RAFT, we use a two-component Laplace mixture for each scalar flow coordinate. Given target y and predicted mean μ, mixture weight $\alpha \in (0, 1)$, and log-scale $\beta \in \mathbb{R}$, the per-coordinate negative log-likelihood is

$$\ell_{\text{mixlap}}(y; \alpha, \beta, \mu) = -\log \left[\frac{\alpha}{2}\, e^{-|y-\mu|} \;+\; \frac{1-\alpha}{2e^{\beta}}\, \exp\!\left(-\frac{|y-\mu|}{e^{\beta}} \right) \right]. \tag{11}$$

For a single optical-flow prediction, the image-level loss sums over spatial locations and the two flow coordinates:

$$\mathcal{L}_{\text{MoL}} = \frac{1}{2HW} \sum_{h=1}^{H} \sum_{w=1}^{W} \sum_{d \in \{x,y\}} \ell_{\text{mixlap}}\big(y_{h,w}^{(d)};\, \alpha_{h,w}, \beta_{h,w}, \mu_{h,w}^{(d)}\big). \tag{12}$$

All parameters (α, β, μ) are predicted per pixel.

B.3 SETTINGS FOR VIDEO PREDICTION.

For a fair comparison, we follow MemFlow (Dong & Fu, 2024): given the last frame $\mathbf{I}_t$, we first predict the forward flow $f_{t\to t+1}$ and a monocular depth map using DPT (Ranftl et al., 2021). We then render a candidate next frame by forward-warping $\mathbf{I}_t$ with Softmax Splatting (Niklaus & Liu, 2020), which yields a splatted image and a disocclusion mask identifying unsupported pixels. Finally, we complete those regions via ZITS inpainting (Dong et al., 2022), producing the synthesized frame $\hat{\mathbf{I}}_{t+1}$.

B.4 CLIP-WISE TRAINING STRATEGY.

Compared to prior mainstream methods, the biggest difference is that our ARFlow keeps the original temporal sequence during the training process. However, most of the previous multi-frame methods, such as MemFlow Dong & Fu (2024) and StreamFlow Sun et al. (2024), interrupt the original temporal sequence by the random training batch shuffle. To be specific, previous methods like MemFlow use the standard batch-wise training strategy, where timestamps among consecutive input batches are not continuous. Thus, their temporal modeling remains constrained to these segments, like 3 frames within one batch, rather than truly covering arbitrary-length sequences because of the shuffled timestamps. This train–test inconsistency cannot reasonably be regarded as effective temporal modeling for long-sequence videos. Furthermore, if the temporal range in one batch is increased, they would suffer from infeasible computational burdens as in Figure 2 of the main manuscript.

In contrast, we treat the whole sequential video clip as input and use a clip-wise training method inspired by MOTR Zeng et al. (2022), rather than the batch-based one. In this case, our memory and supervision can model the temporal information for the whole sequence by sliding along all the frames. Therefore, our temporal receptive field can be viewed as the whole-sequence awareness for each video.

C ADDITIONAL EXPERIMENTS

We also supplement more ablation studies and prediction results here.

Temporal Flow Memory Resolution. We ablate the resolution at which cached flows are stored, comparing $1\times$, $1/4\times$, and $1/16\times$. All models are trained on C+T for fair comparison. As shown in Table 6, storing flows at $1/16\times$ maintains accuracy on Sintel and KITTI while substantially reducing memory. We therefore adopt $1/16\times$ as the default setting in all experiments.

Number of Iterative Refinements (K). Following MEMFOF Bargatin et al. (2025), we vary the number of GRU refinement iterations $K \in \{4, 5, 6, 7, 8\}$ while keeping training on C+T for fairness. As reported in Table 6 (#2), increasing K from 4 to 6 consistently improves Sintel and KITTI metrics. However, increasing to $K{=}7$ or $K{=}8$ yields mixed yet marginal changes (some metrics slightly improve while others slightly degrade), with overall gains being negligible relative to $K{=}6$ and accompanied by higher computation and memory costs. For a balance between speed and accuracy, we choose to perform 6 iterative refinements. For reference, MEMFOF reports using $K = 8$ in their final configuration; since our pipeline builds on MEMFOF as the baseline but benefits from stronger autoregressive initialization and multi-stride forecast fusion, fewer refinement steps suffice in practice.

Pre-trained Temporal Transformer. We replace our Temporal Transformer from our original network with two recent pre-trained Transformer backbones: WAN2.2 (5B) Wan et al. (2025) and Longcat-video (14B) Team et al. (2025). As reported in Table 6 (#3), adding recent pre-trained transformers cannot bring additional performance gains, and our designed temporal transformer already has effective temporal modeling ability.

Sub-sequence Results on Spring Dataset. All the 11 sub-class 1px values on Spring benchmark are listed in Table 7. , where our ARFlow surpasses all recent state-of-the-art methods on most metrics, which demonstrates the excellent performance of our proposed method.

Optical Flow Prediction. We also evaluate the performance in flow prediction in Table 8. Compared to previous methods, ARFlow also achieves the best accuracy in the flow prediction task,

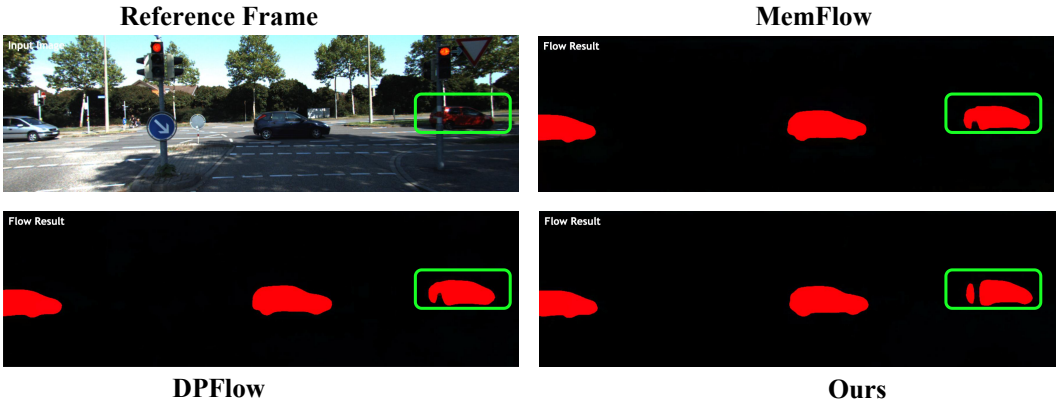

Figure 9: Qualitative results of MemFlow, DPFlow, and our method on the KITTI benchmark with occlusions. Sourced from official leaderboard submissions.

outperforming the recent method MemFlow-P by 10.2%, 13.9%, and 17.8%, respectively, on three datasets. We attribute this great prediction performance to our auto-regressive paradigm, which naturally captures long-range temporal cues and facilitates the flow extrapolation in a frame-by-frame auto-regression manner.

Table 6: **Additional Ablation study.** Settings used as default are underlined. All models are trained on C+T for fair comparison.

Method	Sintel (train)		KITTI-2015 (train)	
	Clean↓	Final↓	EPE↓	F1-all↓
#1: Temporal Flow Memory Resolution				
1	0.90	2.06	2.87	9.27
1/4	0.89	2.09	2.85	9.31
<u>1/16</u>	0.88	2.07	2.86	9.21
#2: The number of iterative refinements (K).				
4	0.90	2.11	2.98	9.89
5	0.88	2.10	2.87	9.35
<u>6</u>	0.88	2.07	2.86	9.21
7	0.88	2.08	2.87	9.20
8	0.89	2.09	2.85	9.23
#3: Pre-trained Transformer				
WAN2.2 (5B) Wan et al. (2025)	0.90	2.08	2.88	9.56
Longcat-video (14B) Team et al. (2025)	0.91	**2.07**	2.89	9.43
<u>w/o pre-trained Transformers</u>	**0.88**	**2.07**	**2.86**	**9.21**

D QUALITATIVE RESULTS ON KITTI, WAYMO AND NUSCENES

We provide additional qualitative comparisons on KITTI, Waymo, and NuScenes datasets.

Visualizations on Occlusions. On KITTI test sequences, our ARFlow produces sharper motion boundaries and better handles occluded regions compared with recent multi-frame methods, as highlighted in Fig. 9. Competing approaches often exhibit artifacts such as blurry edges or incorrect motion in challenging occlusion areas, whereas our autoregressive initialization and multi-stride refinement enable more accurate predictions.

Influence of Different Temporal Lengths. We prove the effectiveness of larger temporal receptive fields by comparing estimation differences on occlusions in Fig. 10. Shortening the temporal modeling length ($T = 4$) leads to much worse estimation accuracy on the occluded signal.

More Visualizations on Spring. We supplement another visualization sample in Fig. 11. From the figure, our estimated flows in the dynamic eyes are more accurate compared to prior methods like MemFlow and StreamFlow.

Table 7: **Sub-sequence Benchmark results on Spring.** The 1px metrics for 11 categories are listed. Best results are respectively highlighted as **first**, second.

	Method	1px in Each Category										
		low-det.	high-det.	matched	unmat.	rigid	non-rig.	not sky	sky	s0-10	s10-40	s40+
NO FINE-TUNE	PWC-Net (Sun et al., 2018b)	82.268	81.747	82.069	90.400	82.817	78.090	81.575	92.761	81.402	82.189	89.693
	FlowNet2 (Ilg et al., 2017b)	6.346	64.061	5.691	48.892	3.711	29.404	6.039	16.908	1.862	5.816	49.693
	RAFT (Teed & Deng, 2020)	6.426	64.087	5.999	39.481	4.107	27.088	5.250	30.183	3.134	5.301	41.403
	GMA (Jiang et al., 2021)	6.699	66.203	6.281	39.892	4.276	28.247	5.614	29.263	3.645	5.389	40.327
	GMFlow (Xu et al., 2022)	9.935	76.613	9.060	63.949	6.800	37.258	8.952	31.680	5.412	9.901	52.944
	FlowFormer (Huang et al., 2022)	6.144	64.219	5.766	37.294	3.527	29.084	5.500	21.858	3.381	5.530	35.344
	MemFlow (Dong & Fu, 2024)	5.394	63.348	5.107	32.755	3.293	24.422	4.494	24.990	2.918	4.820	32.071
	StreamFlow (Sun et al., 2024)	4.869	59.550	4.559	32.343	2.865	22.987	4.435	17.059	2.597	4.492	29.067
	MEMFOF (Bargatin et al., 2025)	3.254	58.072	3.049	26.384	**1.510**	19.416	3.708	**1.961**	1.315	4.574	20.081
	ARFlow (Ours)	**3.180**	**57.251**	**2.973**	**26.375**	1.675	**17.526**	**3.395**	5.505	**1.084**	**4.244**	**22.009**
FINE-TUNE	CrocoFlow (Weinzaepfel et al., 2023)	4.209	60.594	3.848	34.200	2.194	22.501	4.479	5.868	1.225	4.332	33.134
	SEA-RAFT (S) (Wang et al., 2024b)	3.536	61.951	3.172	34.228	1.662	20.871	3.974	2.855	1.264	4.871	23.378
	SEA-RAFT (M) (Wang et al., 2024b)	3.323	60.986	3.025	31.058	1.561	19.769	3.757	2.616	1.241	4.760	21.237
	MemFlow (Dong & Fu, 2024)	4.119	61.703	3.742	35.115	2.391	20.306	3.934	12.809	1.305	4.437	31.184
	StreamFlow (Sun et al., 2024)	3.790	61.297	3.424	34.304	1.986	20.544	3.986	6.678	1.236	4.381	27.935
	DPFlow (Morimitsu et al., 2025)	3.102	56.941	2.859	27.563	1.500	18.132	3.522	**2.218**	1.188	**3.998**	20.786
	MEMFOF (Bargatin et al., 2025)	2.947	57.246	2.751	**25.551**	1.446	17.236	3.327	2.723	1.084	4.202	19.270
	ARFlow (Ours)	**2.926**	**56.655**	**2.717**	25.955	**1.436**	**17.108**	**3.325**	2.362	**1.079**	4.160	**19.133**

Table 8: **End-point-error of flow prediction on FlyingThings3D (Final) Mayer et al. (2016), Sintel (Final), and KITTI-15.**

Method	FlyingThings3D (Final)	Sintel (Final)	KITTI-15
Warped Oracle	14.76	5.76	-
MemFlow Dong & Fu (2024)	15.70	6.23	12.95
OFNet Ciamarra et al. (2022)	13.76	6.03	12.43
MemFlow-P Dong & Fu (2024)	7.56	5.38	8.82
Ours	**6.79**	**4.63**	**7.25**

Zero-shot Generalization on Waymo and Nuscenes. Moreover, we visualize zero-shot generalization on Waymo (Sun et al., 2020) and NuScenes (Caesar et al., 2020). Importantly, these datasets are not used during training, yet our ARFlow still achieves high-quality optical flow predictions. As shown in Fig. 12, Fig. 13, Fig. 14, and Fig. 15, our method maintains robust performance in diverse driving scenarios, confirming its strong generalization ability beyond the training distributions.

E Screenshots for Benchmark results on KITTI, Sintel, and Spring

We include official benchmark screenshots for KITTI-15, Spring, and Sintel in Fig. 16, Fig. 17, and Fig. 18, retrieved on September 23, 2025 (KITTI-15 and Spring) and September 25, 2025 (Sintel).

On *KITTI-15 (Geiger et al., 2013)*, ARFlow ranks **first among all optical flow methods**, achieving the best results on both All and Non-Occ pixels. Note that methods ranked above ours on the leaderboard mainly rely on scene flow or additional 3D information rather than pure optical flow.

On the *Spring* benchmark (Mehl et al., 2023b), ARFlow ranks **first among all open-source methods**, surpassing strong baselines such as MEMFOF and DPFlow.

For *Sintel* (Butler et al., 2012), our method achieves **second place among open-source methods**, matching or outperforming recent state-of-the-art approaches.

These results consistently highlight the advantages of our autoregressive paradigm: scalable temporal modeling, reliable initialization, and robust refinement across datasets.

F LLM Usage Statement

A large language model (ChatGPT) was used in a strictly limited assistive manner during manuscript preparation. Its usage was confined to: (i) spelling and grammatical error checking; (ii) minor phrasing and wording refinement to improve fluency without altering technical meaning, methodology, analyses, or conclusions; and (iii) occasional condensation of repetitive sentences and suggestions

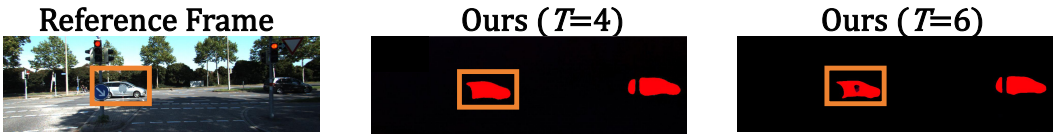

Figure 10: Qualitative results of different temporal lengths on the KITTI benchmark. Sourced from official leaderboard submissions.

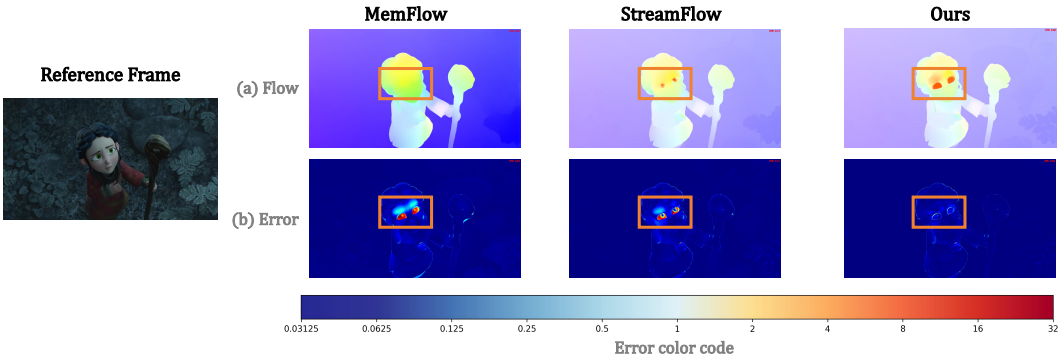

Figure 11: Qualitative results on the Spring benchmark.

for consistent formatting. The LLM did not contribute to research ideation, problem formulation, method design, experimental execution, data processing, result analysis, drafting of technical content, or formulation of conclusions. The LLM is not an author and bears no responsibility for the content.

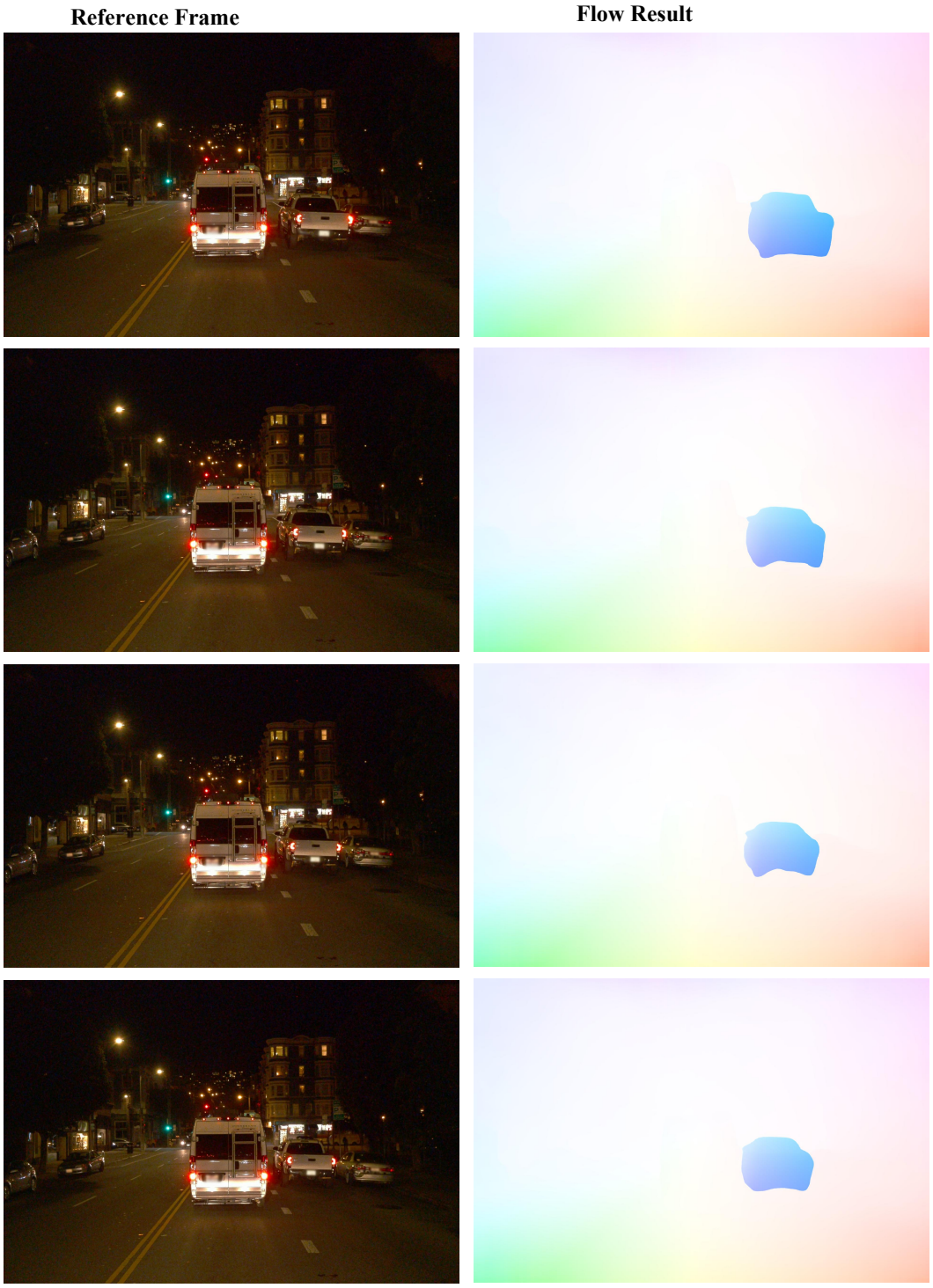

Figure 12: Qualitative results of our method on the Waymo dataset (Sun et al., 2020) (1). Note that our model was not trained on the Waymo dataset.

Figure 13: Qualitative results of our method on the Waymo dataset (Sun et al., 2020) (2). Note that our model was not trained on the Waymo dataset.

Figure 14: Qualitative results of our method on the NuScenes dataset (Caesar et al., 2020) (1). Note that our model was not trained on the NuScenes dataset.

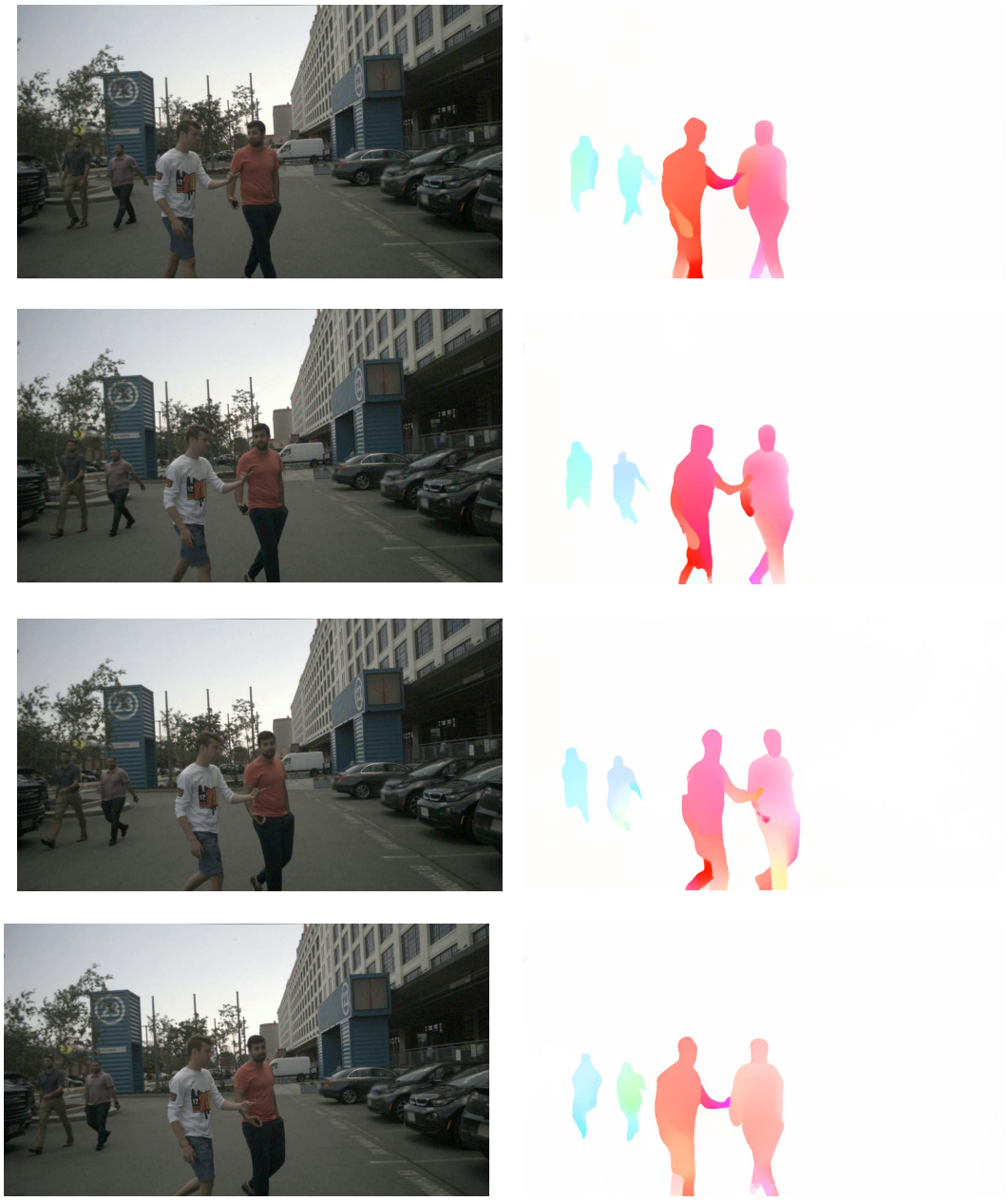

Figure 15: Qualitative results of our method on the NuScenes dataset (Caesar et al., 2020) (2). Note that our model was not trained on the NuScenes dataset.

The KITTI Vision Benchmark Suite
A project of Karlsruhe Institute of Technology and Toyota Technological Institute at Chicago

home | setup | stereo | flow | sceneflow | depth | odometry | object | tracking | road | semantics | raw data | submit results

A. Geiger | P. Lenz | C. Stiller | R. Urtasun — Log in

Optical Flow Evaluation 2015

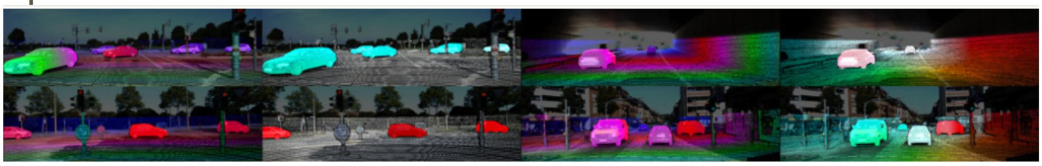

The **stereo 2015 / flow 2015 / scene flow 2015** benchmark consists of 200 training scenes and 200 test scenes (4 color images per scene, saved in loss less png format). Compared to the stereo 2012 and flow 2012 benchmarks, it comprises dynamic scenes for which the ground truth has been established in a semi-automatic process. Our evaluation server computes the percentage of bad pixels averaged over all ground truth pixels of all 200 test images. For this benchmark, we consider a pixel to be correctly estimated if the disparity or flow end-point error is **<3px or <5%** (for scene flow this criterion needs to be fulfilled for both disparity maps and the flow map). We require that all methods use the same parameter set for all test pairs. Our development kit provides details about the data format as well as MATLAB / C++ utility functions for reading and writing disparity maps and flow fields. More details can be found in Object Scene Flow for Autonomous Vehicles (CVPR 2015).

Evaluation ground truth: All pixels — Evaluation area: All pixels

	Method	Setting	Code	Fl-bg	Fl-fg	Fl-all	Density	Runtime	Environment	Compare
1	SEA-Flow3D + Monster			**1.98 %**	5.30 %	**2.53 %**	100.00 %	0.07 s	GPU @ 2.5 Ghz (Python)	
2	MS-RAFT-3D+		code	2.22 %	5.99 %	2.85 %	100.00 %	3 s	GPU @ 2.5 Ghz (Python)	
	J. Schmid, A. Jahedi, N. Senn and A. Bruhn: MS-RAFT-3D: A Multi-Scale Architecture for Recurrent Image-Based Scene Flow. IEEE International Conference on Image Processing (ICIP) 2025.									
3	ARFlow			2.48 %	4.69 %	2.85 %	100.00 %	0.35 s	GPU @ 2.5 Ghz (Python)	
4	SplatFlow3D		code	2.27 %	6.02 %	2.89 %	100.00 %	0.1 s	1 core @ 2.5 Ghz (Python)	
	B. Wang, Y. Zhang, J. Li, Y. Yu, Z. Sun, L. Liu and D. Hu: SplatFlow: Learning Multi-frame Optical Flow via Splatting. International Journal of Computer Vision 2024.									
5	SEA-Flow3D+gannet			2.08 %	6.95 %	2.89 %	100.00 %	0.07 s	1 core @ 2.5 Ghz (Python)	
6	OAMaskFlow			2.07 %	7.11 %	2.91 %	100.00 %	0.5 s	1 core @ 2.5 Ghz (Python)	
7	MEMFOF		code	2.60 %	4.66 %	2.94 %	100.00 %	0.4 s	GPU @ 2.5 Ghz (Python)	
	V. Bargatin, E. Chistov, A. Yakovenko and D. Vatolin: MEMFOF: High-Resolution Training for Memory-Efficient Multi-Frame Optical Flow Estimation. arXiv preprint arXiv:2506.23151 2025.									
8	CamLiRAFT		code	2.08 %	7.37 %	2.96 %	100.00 %	1 s	GPU @ 2.5 Ghz (Python + C/C++)	
	H. Liu, T. Lu, Y. Xu, J. Liu and L. Wang: Learning Optical Flow and Scene Flow with Bidirectional Camera-LiDAR Fusion. TPAMI 2023.									
9	CamLiFlow		code	2.31 %	7.04 %	3.10 %	100.00 %	1.2 s	GPU @ 2.5 Ghz (Python + C/C++)	
	H. Liu, T. Lu, Y. Xu, J. Liu, W. Li and L. Chen: CamLiFlow: Bidirectional Camera-LiDAR Fusion for Joint Optical Flow and Scene Flow Estimation. CVPR 2022.									
10	DDVM			2.90 %	5.05 %	3.26 %	100.00 %			
	S. Saxena, C. Herrmann, J. Hur, A. Kar, M. Norouzi, D. Sun and D. Fleet: The Surprising Effectiveness of Diffusion Models for Optical Flow and Monocular Depth Estimation. NeurIPS 2023.									
11	WAFTv2-DAv2			2.98 %	4.94 %	3.31 %	100.00 %	0.24 s	NVIDIA RTX3090	
12	TDFlow			3.00 %	5.06 %	3.34 %	100.00 %	0.1 s	GPU @ 2.5 Ghz (Python)	
13	DF			3.05 %	5.23 %	3.42 %	100.00 %	0.1 s	1 core @ 2.5 Ghz (C/C++)	
14	CamLiRAFT-NR		code	2.76 %	6.78 %	3.43 %	100.00 %	1 s	GPU @ 2.5 Ghz (Python + C/C++)	
	H. Liu, T. Lu, Y. Xu, J. Liu and L. Wang: Learning Optical Flow and Scene Flow with Bidirectional Camera-LiDAR Fusion. arXiv preprint arXiv:2303.12017 2023.									
15	PAFlow			2.75 %	6.86 %	3.43 %	100.00 %	0.53 s	1 core @ 2.5 Ghz (C/C++)	
16	M-FUSE		code	2.66 %	7.47 %	3.46 %	100.00 %	1.3 s	GPU	

Figure 16: Screenshots from the KITTI-15 optical flow benchmark on the official website, retrieved on September 23, 2025. **Note:** The methods ranked above ours are based on **scene flow** rather than optical flow.

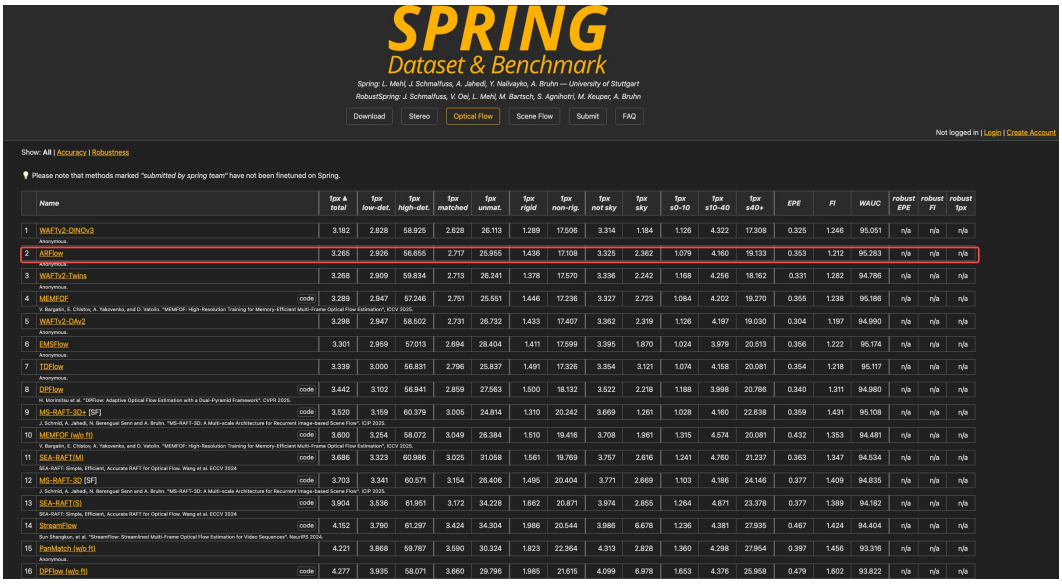

	Name	1px & total	1px low-det.	1px high-det.	1px matched	1px unmat.	1px rigid	1px non-rig.	1px not sky	1px sky	1px s0-10	1px s10-40	1px s40+	EPE	Fl	WAUC	robust EPE	robust Fl	robust 1px
1	WAFTv2-DINOv3 Anonymous.	3.182	2.828	58.925	2.628	26.113	1.289	17.506	3.314	1.184	1.126	4.322	17.308	0.325	1.246	95.051	n/a	n/a	n/a
2	ARFlow Anonymous.	3.265	2.926	56.655	2.717	25.955	1.436	17.108	3.325	2.362	1.079	4.160	19.133	0.353	1.212	95.283	n/a	n/a	n/a
3	WAFTv2-Twins Anonymous.	3.268	2.909	59.834	2.713	26.241	1.378	17.570	3.336	2.242	1.168	4.256	18.162	0.331	1.282	94.786	n/a	n/a	n/a
4	MEMFOF code V. Bargatin, E. Chistov, A. Yakovenko, and D. Vatolin. "MEMFOF: High-Resolution Training for Memory-Efficient Multi-Frame Optical Flow Estimation", ICCV 2025.	3.289	2.947	57.246	2.751	25.551	1.446	17.236	3.327	2.723	1.084	4.202	19.270	0.355	1.238	95.186	n/a	n/a	n/a
5	WAFTv2-DAv2 Anonymous.	3.298	2.947	58.502	2.731	26.732	1.433	17.407	3.362	2.319	1.126	4.197	19.030	0.304	1.197	94.990	n/a	n/a	n/a
6	EMSFlow Anonymous.	3.301	2.959	57.013	2.694	28.404	1.411	17.599	3.395	1.870	1.024	3.979	20.513	0.356	1.222	95.174	n/a	n/a	n/a
7	TDFlow Anonymous.	3.339	3.000	56.831	2.796	25.837	1.491	17.326	3.354	3.121	1.074	4.158	20.081	0.354	1.218	95.117	n/a	n/a	n/a
8	DPFlow code N. Morrical et al., "DPFlow: Adaptive Optical Flow Estimation with a Dual-Pyramid Framework", CVPR 2025.	3.442	3.102	56.941	2.859	27.563	1.500	18.132	3.522	2.218	1.188	3.998	20.786	0.340	1.311	94.980	n/a	n/a	n/a
9	MS-RAFT-3D+ [SF] J. Schmid, A. Jahedi, N. Berenguel Senn and A. Bruhn. "MS-RAFT-3D: A Multi-scale Architecture for Recurrent Image-based Scene Flow", ICIP 2025.	3.520	3.159	60.379	3.005	24.814	1.310	20.242	3.669	1.261	1.028	4.160	22.638	0.359	1.431	95.108	n/a	n/a	n/a
10	MEMFOF (wfo ft) code V. Bargatin, E. Chistov, A. Yakovenko, and D. Vatolin. "MEMFOF: High-Resolution Training for Memory-Efficient Multi-Frame Optical Flow Estimation", ICCV 2025.	3.600	3.254	58.072	3.049	26.384	1.510	19.416	3.708	1.961	1.315	4.574	20.081	0.432	1.353	94.481	n/a	n/a	n/a
11	SEA-RAFT(M) code SEA-RAFT: Simple, Efficient, Accurate RAFT for Optical Flow. Wang et al. ECCV 2024	3.686	3.323	60.986	3.025	31.058	1.561	19.769	3.757	2.616	1.241	4.760	21.237	0.363	1.347	94.534	n/a	n/a	n/a
12	MS-RAFT-3D [SF] code J. Schmid, A. Jahedi, N. Berenguel Senn and A. Bruhn. "MS-RAFT-3D: A Multi-scale Architecture for Recurrent Image-based Scene Flow", ICIP 2025.	3.703	3.341	60.571	3.154	26.406	1.495	20.404	3.771	2.669	1.103	4.186	24.146	0.377	1.409	94.835	n/a	n/a	n/a
13	SEA-RAFT(S) code SEA-RAFT: Simple, Efficient, Accurate RAFT for Optical Flow. Wang et al. ECCV 2024	3.904	3.536	61.951	3.172	34.228	1.662	20.871	3.974	2.855	1.264	4.871	23.378	0.377	1.389	94.182	n/a	n/a	n/a
14	StreamFlow code Sun Shangkun, et al. "StreamFlow: Streamlined Multi-Frame Optical Flow Estimation for Video Sequences". NeurIPS 2024.	4.152	3.790	61.297	3.424	34.304	1.986	20.544	3.986	6.678	1.236	4.381	27.935	0.467	1.424	94.404	n/a	n/a	n/a
15	PanMatch (wfo ft) Anonymous.	4.221	3.868	59.787	3.590	30.324	1.823	22.364	4.313	2.828	1.360	4.298	27.954	0.397	1.456	93.316	n/a	n/a	n/a
16	DPFlow (wfo ft) code	4.277	3.935	58.071	3.660	29.796	1.985	21.615	4.099	6.978	1.653	4.376	25.958	0.479	1.602	93.822	n/a	n/a	n/a

Figure 17: Screenshots from the Spring optical flow benchmark on the official website, retrieved on September 23, 2025. **Note:** To the best of our knowledge (as of September 23, 2025), *WAFTv2* does not have a publicly available paper.

Final | Clean

	EPE all	EPE matched	EPE unmatched	d0-10	d10-60	d60-140	s0-10	s10-40	s40+	
GroundTruth [1]	0.000	0.000	0.000	0.000	0.000	0.000	0.000	0.000	0.000	Visualize Results
ViCo_VideoFlow_MOF [2]	1.618	0.768	8.543	1.966	0.601	0.348	0.392	1.198	8.705	Visualize Results
CFFlow [3]	1.647	0.788	8.650	2.087	0.609	0.334	0.402	1.242	8.793	Visualize Results
VideoFlow-MOF [4]	1.649	0.788	8.660	2.090	0.609	0.334	0.403	1.243	8.804	Visualize Results
TSA_ [5]	1.652	0.794	8.645	1.881	0.667	0.445	0.391	1.090	9.264	Visualize Results
MemoFlow [6]	1.692	0.805	8.917	2.125	0.631	0.338	0.407	1.262	9.098	Visualize Results
VideoFlow-BOF [7]	1.713	0.812	9.054	2.056	0.636	0.387	0.387	1.242	9.422	Visualize Results
ARFlow [8]	1.786	0.805	9.789	2.102	0.618	0.390	0.312	1.104	10.749	Visualize Results
sdex001 [9]	1.824	0.908	9.270	2.446	0.682	0.421	0.416	1.424	9.746	Visualize Results
MemFlow-T [10]	1.840	0.874	9.710	2.233	0.671	0.370	0.467	1.351	9.828	Visualize Results
StreamFlow [11]	1.874	0.824	10.435	2.091	0.635	0.350	0.409	1.240	10.674	Visualize Results
GeoViT [12]	1.883	0.961	9.390	1.746	0.622	0.696	0.329	1.092	11.501	Visualize Results
MEMFOF-XL [13]	1.890	0.863	10.257	2.092	0.634	0.496	0.319	1.131	11.513	Visualize Results
MEMFOF-L [14]	1.907	0.877	10.302	2.101	0.637	0.512	0.324	1.128	11.644	Visualize Results
MemFlow [15]	1.914	0.931	9.928	2.332	0.736	0.419	0.430	1.382	10.556	Visualize Results
SemFlow-2view [16]	1.925	0.902	10.265	2.376	0.768	0.359	0.445	1.366	10.622	Visualize Results
MEMFOF [17]	1.942	0.890	10.513	2.121	0.641	0.524	0.332	1.125	11.900	Visualize Results

Figure 18: Screenshots from the Sintel optical flow benchmark on the official website, retrieved on September 25, 2025. **Note:** To the best of our knowledge (as of September 25, 2025), only *VideoFlow* has a publicly available paper; the other higher-ranked methods do not have publicly available publications.